Title: Pontine reticulospinal projections in the neonatal mouse – internal organization and axon trajectories

Authors: Magne S. Sivertsen[1], Marie-Claude Perreault[2] and Joel C. Glover[1,3]

Affiliations: 1. Laboratory of Neural Development and Optical Recording (NDEVOR), Department of Physiology, Institute of Basic Medical Sciences, Faculty of Medicine, University of Oslo, Oslo, Norway. 2. Department of Physiology, Emory University School of Medicine, Atlanta, USA. 3. Norwegian Center for Stem Cell Research, Oslo University Hospital, Oslo, Norway

Running Head: Pontine reticulospinal projections in newborn mouse

Associate Editor: Gert Holstege

Key words: Descending Pathways, Brainstem, Spinal Cord, Motor Control, Bulbospinal, Startle Reflex, Posture, Locomotion, AB 1502299, AB 10143907, AB 141784

Address for Correspondence: Joel C. Glover, Laboratory of Neural Development and Optical Recording (NDEVOR), Department of Physiology, Institute of Basic Medical Sciences, University of Oslo, PB 1103 Blindern, Oslo, Norway. Telephone: +47-22851230; E-mail: joel.glover@medisin.uio.no

Grant support: Supported by grants from the Norwegian Research Council and the University of Oslo (JCG) and from the South-East Norway Regional Health Authority (MCP).

Abstract *(249 words)*

We recently characterized the pontine reticulospinal (pRS) projection in the neonatal mouse physiologically, and showed that it mediates synaptic effects on spinal motoneurons via parallel uncrossed and crossed pathways (Sivertsen et al 2014). Here, we have characterized the origins, anatomical organization and axon trajectories of these pathways using retrograde axonal tracing with conjugated dextran-amines. The uncrossed and crossed pathways derive from segregated populations of ipsilaterally and contralaterally projecting pRS neurons with characteristic locations within the pontine reticular formation (PRF). Ipsilateral pRS neurons outnumber contralateral pRS neurons by a factor of about 3, and are roughly equally divided between rostral and caudal regions of the PRF, whereas contralateral pRS neurons are concentrated in the rostral PRF. Ipsilateral pRS neuron cell bodies are on average larger than contralateral, with a regionally systematic variation in which more caudal and more ventral ipsilateral pRS neurons are largest. The pRS neurons are interspersed with putative GABAergic interneurons. The axons from the ipsilateral and contralateral pRS populations follow distinctly different trajectories within the brainstem. On entering the spinal cord, there is a differential, graded distribution of pRS axons within the white matter, such that ipsilateral and contralateral pRS axons are more highly concentrated medially and laterally, respectively. The larger size and number of ipsilateral versus contralateral pRS neurons is compatible with our previous finding that the uncrossed projection transmits more reliably to spinal motoneurons. The new information about pRS axon trajectories will facilitate the physiological assessment of synaptic connections between pRS neurons and spinal interneurons.

Introduction

Most descending projections to the spinal cord in mammals arise from the brainstem (24 out of 27 neuron groups of origin, Nudo and Masterton, 1988; over 70% of projecting neurons, Liang et al 2011). Although descending projections from the brainstem are heavily involved in the control of sensory, autonomic and motor functions, how this control is achieved is poorly understood. One important gap in our knowledge involves the internal organization of brainstem descending projection neuron groups into subpopulations according to different functional phenotypes and axon trajectories within the brainstem and spinal cord.

Brainstem projections to the spinal cord begin to develop prenatally and many have established contact with potential target neurons in the spinal cord by birth (Perreault and Glover, 2013). Several lines of evidence suggest that during development the brainstem sources of these projections are internally patterned by regionally differentiated gene expression, and that this patterning gives rise to heterogeneity in axon projections and synaptic targeting (Diaz et al 1998; Auclair et al 1999; Glover, 2000; Cepeda-Nieto et al., 2005; Pasqualetti et al., 2007; Perreault and Glover, 2013). Thus, characterization of these projections in neonates is likely to reveal key features of internal organization that relate to functional connectivity.

We recently characterized in the neonatal mouse the pattern of functional connections between pontine reticulospinal (pRS) neurons and spinal motoneurons (MNs), using optical recording of synaptically mediated calcium responses (Sivertsen et al., 2014). We showed that these connections are already established at birth and are mediated by two parallel channels, one involving pRS axons that descend ipsilaterally (uncrossed projection) and the other involving pRS axons that descend contralaterally (crossed projection). While the ipsilateral projection transmits more faithfully and may be more direct, both pRS projections elicit responses in axial and limb MNs in cervical, thoracic and lumbar levels, suggesting that both are involved in coordinating widespread patterns of muscle activation.

This organization into different parallel channels has prompted us to make a more precise analysis of the internal organization of the pRS neuron population, with a particular focus on comparing the anatomical locations of the ipsilaterally- and contralaterally-projecting pRS neurons (hereafter referred to as “ipsilateral” and “contralateral” pRS neurons) and their axon trajectories to the spinal cord. We find that ipsilateral pRS neurons are about three times more numerous than contralateral, and that the two populations are differentially distributed within the PRF. Ipsilateral pRS neurons are equally divided between regions corresponding to the oral and caudal pontine reticular nuclei (PnO and PnC) whereas contralateral pRS neurons are more concentrated within the PnO. The two populations are also spatially segregated within the transverse plane, with the contralateral pRS neuron population occupying a domain just ventrolateral to the ipsilateral. The two populations of pRS axons project along distinct trajectories within the brainstem, and as they enter the spinal cord they have an

oppositely graded mediolateral distribution within the white matter. Ipsilateral pRS axons are more concentrated medially, within the ventral funiculus (VF), whereas contralateral pRS axons are more concentrated laterally, within the lateral funiculus (LF). Part of this work has been published previously in abstract form (Sivertsen et al., 2013).

Methods

Animals

Experiments were performed on preparations of the brainstem and cervical spinal cord from wild-type mice of the Hsd:ICR (CD-1) strain (Harlan, France; n=20, all P0 except for one P2 mouse that was used for neurofilament immunohistochemistry) or the transgenic strains GAD-67 (Tamamaki et al, 2003; P1, n=2) and GIN ("GFP-expressing Inhibitory Neurons", Oliva et al 2000; Jackson strain FVB-Tg(GadGFP)45704Swn/J; P0, n=2). After deep inhalation anaesthesia with isoflurane and a craniotomy, pups were decerebrated by transecting the brain between the superior colliculus and the forebrain and then submerged in ice-cold (4°C), oxygenated (95% O2 and 5% CO2), low calcium, "dissection" artificial cerebrospinal fluid (d-ACSF, containing in mM: glycerol 250, KCl 2, d-glucose 11, CaCl2 0.15, MgSO4 2, NaH2PO4 1.2, HEPES 5, and NaHCO3 25). Animals were then eviscerated and the brainstem together with cervical and upper thoracic spinal cord was carefully dissected out. To maximize oxygenation the cerebellum was removed and the d-ACSF was exchanged every 5 min during the dissection.

All efforts were made to minimize the number of animals used and their suffering in accordance with the European Communities Council directive 86/609/EEC and the National Institutes of Health guidelines for the care and use of animals. All procedures were approved by the Norwegian National Animal Research Authority.

Retrograde labeling of pRS neurons

After transfer of the preparations to room temperature, oxygenated artificial cerebrospinal fluid (ACSF, containing in mM: NaCl 128, KCl 3, d-glucose 11 CaCl2 2.5, MgSO4 1, NaH2PO4 1.2, HEPES 5 and NaHCO3 25), the spinal white matter at the level of the second cervical (C2) ventral root was cut unilaterally. The cut spanned the entire extent of the ventral and lateral funiculi (VF+LF) or more restricted regions thereof (defined below). To ensure that the LF was included in its entirety, the cut extended beyond the dorsal limit of the LF into the dorsolateral funiculus (DLF). Pre-made crystals of 3 kDa tetramethylrhodamine-conjugated dextran amines (RDA, Invitrogen, catalog number D-3308), alone or in combination (ratio 1:1) with biotin-conjugated dextran amine (BDA, Invitrogen, catalog number D-7135) were inserted into the cut (Glover et al., 1986). Four to ten crystals inserted over a period of about 3 min ensured continuous exposure of the cut axons to high tracer concentration. Preparations were then incubated in the dark for a period of about 12 hours to allow retrograde transport of the tracers to both ipsilaterally- and contralaterally-projecting pRS neurons.

To eliminate the possibility of contamination by unintentional labeling of contralateral axons, in all but one preparation the contralateral spinal cord between C1 and T1 was carefully removed prior to

application of RDA/BDA. All application sites and lesions were assessed histologically at the end of the experiment (see below).

Retrograde labeling of restricted subpopulations of pRS axons

To characterize the funicular trajectories of pRS axons, in 9 preparations we restricted RDA/BDA application to one of three zones of the VF+LF white matter by making smaller cuts of defined circumferential extent. The three zones, denoted Zones 1, 2 and 3 from medial to lateral, were of roughly equal size. Zone 1 extended from the midline to the ventral apex of the hemicord, and thus encompassed the medial part of the VF. Zone 2 extended from the ventral apex of the hemicord to the longitudinal line along which ventral roots exited the spinal cord ("ventral root line"), and thus encompassed the lateral part of the VF and possibly a small part of the LF. Zone 3 extended from the ventral root line to just beyond the dorsal margin of the LF. All application sites were assessed histologically at the end of the experiment (see below).

Histology and immunohistochemistry

After each labeling experiment, the preparations were fixed with 4% paraformaldehyde in phosphate buffered saline (PBS) for 4 h, cryoprotected in 20% sucrose in PBS (4-24 h) and separated into brainstem and spinal cord portions. These were separately embedded in OCT (Tissue-Tek), frozen and cryostat-sectioned, either in a single series of 50µm thick sections in the parasagittal, horizontal or transverse plane (brainstem portion) or transverse plane (spinal cord portion), or in an alternating series of 14µm thick sections in the transverse plane (for 3D reconstruction of the brainstem portion, see below). Before further analysis, all spinal cord application sites and lesions were examined histologically for completeness. Their extents were evaluated through comparison with a standard cervical cord section and preparations that differed from the intended extent by more than 20% in either direction were discarded. Immunohistochemistry for neurofilaments (Table 1) was performed on 12µm transverse sections from a spinal cord not subjected to retrograde labeling.

The transverse 50µm sections through the spinal cord and one of the two alternating series of 14µm transverse sections through the brainstem were stained with methylene blue (Difco Laboratories, West Molesey, Surrey, UK; 10-20 s in 0.3% w/v solution). The second alternating series of 14µm transverse sections through nine brainstems (n=3 for VF+LF, n=2 for each of Zones 1, 2 and 3) were subjected to fluorescent signal enhancement. The combined RDA/BDA labeling was enhanced using either an anti-rhodamine antibody (Table 1) and a red fluorophore-conjugated secondary antibody (Alexa 555 goat-anti-rabbit IgG, Invitrogen, Table 1), or a red fluorophore-conjugated streptavidin (Cy3-Streptavidin, Jackson Laboratories, catalog number 016-220-084). The signal enhancement achieved by the two

methods was comparable, and in both cases much improved compared to the non-enhanced signal. The enhancement made detection of labeled somata more reliable, and greatly improved the visualization of labeled neurites (both axons and dendrites).

All sections were cover-slipped in gelatin-glycerol (50% v/v glycerol and 20% w/v gelatin in PBS), and photographed using a ProgRes C14 215 camera (Jenoptik) mounted on an AX70 microscope (Olympus) using 4x (UplanApo, NA 0.16) or 10x (UplanApo, NA 0.40) objectives. Selected sections were also imaged with a laser scanning confocal microscope (Z-stacks obtained using a Zeiss LSM Pascal 5 confocal microscope at 20x magnification, PLAN APOCHROMAT, NA 0.75)).

Spatial distribution maps, soma sizes and neuron density

To estimate pRS neuron soma size and relate it to position within the PRF, we used two of the VF+LF labeled brainstems sectioned at 50µm in the parasagittal plane to construct spatial distribution maps. Confocal projection images were opened in ImageJ (U.S. National Institutes of Health, Bethesda, MD, USA; http://rsb.info.nih.gov/ij/), and a plug-in was used to trace the outline of labeled neurons. The outlines were submitted to a program written in Python (http://www.python.org) for computation of the neuron area (ParticleDensityDouble; Max Larsson 2014). The source code of the ImageJ plug-in and the Python program are available online http://www.hu.liu.se/forskning/larsson-max/software?l=en, NIH, open access). In a drawing program (CorelDraw4x, v14.0) a 2D matrix of 10µm squares was superimposed onto 4x images of the sections and aligned using specific landmarks, so that each soma could be assigned rostrocaudal and dorsoventral coordinates. Section number was used to define the mediolateral coordinate. To calculate neuron densities, we applied a grid of 100µm-sided cubes onto the Excel coordinate database, counting the number of labeled neurons within each cube.

3D reconstructions

Nine brainstems (n=3 for VF+LF, n=2 for each of Zones 1, 2 and 3) were sectioned at 14µm in alternating series of which one was labeled with methylene blue and the other subjected to fluorescent signal enhancement as described above. Every sixth section in these two series was photographed using a Zeiss Axioskop2 microscope equipped with a motorized stage (Märzhäuser), a CX9000 camera (MBF) and a 10x objective (Achroplan, NA 0.25). Images were imported into Neurolucida software (Version 8, MBF, USA), and specific section features (section outline and midline in all sections, outlines of distinguishable nuclei based on Paxinos et al (2007) in one section series, and RDA/BDA-labeled neuronal somata in the other section series) were digitally traced or marked. Marked neurons were also given a digital name tag based on comparison to the structures mapped in the immediately adjacent methylene blue-labeled section, falling into one of the pRS neuron

populations defined in Results. The alternating digital section series were then intercalated, allowing the construction of digital 3D models. In the 3D models, the anteroposterior extent of the pRS neuron population spanned about 12-13 digitized transverse sections. Because the angle we used for the transverse sections was not identical to that used by Paxinos et al. (2007) (partly because our material was sectioned after dissection and ex vivo incubation, which permits a more accurate alignment of the rostrocaudal axis), for presentation purposes outlines of cytoarchitectonically defined structures and nuclei were produced based on section-by-section comparison of our series with the series in Paxinos et al. (2007). Interpolation between multiple sections from the Paxinos et al. (2007) series was used where necessary to obtain appropriate outlines that could be superimposed on our sections (see Figure 2).

Neuron numbers and densities

To estimate the number of neurons within the pRS neuron subpopulations, two different procedures were used. In one, we multiplied the number of marked ipsilateral and contralateral pRS neurons compiled in every sixth 14µm section of the 3D reconstructions (described above) by 6. We did not correct for potential errors due to "double-counting" of neurons intersected by a section plane (see Discussion). In the other, we simply counted all the soma outlines that were drawn in the parasagittal 50µm sections used for spatial distribution maps.

Statistics

Data analysis was performed in Excel or the statistics software SPSS (IBM, USA). All graphs and plots were produced in SPSS. Distributions are presented as mean plus/minus standard deviation, where applicable, or range when n equaled 2.

Results

The pRS neurons and their axons were retrogradely labeled unilaterally from the spinal C2 segment in isolated brainstem-spinal cord preparations from 19 newborn (P0) mice (Figure 1A). In 10 preparations the white matter encompassing the VF and LF was labeled in its entirety on one side. In the remaining 9 preparations, retrograde labeling was restricted to one of 3 zones that divided the combined VF+LF into equal parts (Zones 1-3, Figure 1B-D). To ensure that the LF was labeled throughout its dorsal extent we always extended the application site into the dorsolateral funiculus (DLF, arrow in Figure 1B-C; Sengul et al., 2012) in VF+LF and in Zone 3 preparations. Three VF+LF preparations and two each of the Zone 1, 2 and 3 preparations were used for 3D reconstructions. Two VF+LF preparations were used for neuron size, density and spatial distribution analysis. The remaining preparations were used for qualitative anatomical analyses.

General spatial distribution of ipsilaterally and contralaterally projecting pRS neurons

Retrogradely labeled neurons were found in several regions of the pons, including those corresponding in Paxinos et al (2007) to the nucleus reticularis pontis pars oralis (PnO) and pars caudalis (PnC), the locus coeruleus (LC), the nucleus subcoeruleus (SubCA), the vestibular nuclei, and some structures and areas adjacent to these (Figure 2). Here we focus only on the neurons labeled retrogradely within the region corresponding to the pontine reticular nuclei (PnC and PnO) together with small numbers of neurons clearly contiguous with these and not associated with other distinct labeled neuron clusters nearby. We define these neurons collectively as the pRS neuron population. In the description that follows, we describe the pRS neuron population in a series of 4 transverse sections moving from rostral to caudal (Figure 2A-D), taken from a representative preparation. To provide anatomical orientation, we have superimposed boundaries of specific nuclei and axon tracts onto each section (see Materials and Methods for a detailed description of how this was done). However, we wish to emphasize that such delineation of specific neuroanatomical structures is by its very nature subjective and should therefore be interpreted with caution.

In the most rostral section (Figure 2A), we found labeled pRS neurons both ipsilateral and contralateral to the tracer application site, beginning at about the same rostral level. The ipsilateral pRS neurons were located dorsolaterally within the area corresponding to the PnO. The contralateral pRS neurons were located ventrolaterally, having a center of density just inside the presumed PnO border, with some found on either side of this border.

Moving caudally (Figure 2B), the ipsilateral pRS neuron population broadened dorsoventrally so that it occupied the whole lateral half of the PnO. Some ipsilateral pRS neurons were located outside the presumed ventrolateral border of the PnO, close to and sometimes among the labeled axons of the

rubrospinal (rs) tract (Figure 2B). At this level, a few labeled neurons were also found within the ipsilateral subcoeruleus nucleus, alpha part (SubCA). As defined above, we did not consider these labeled neurons to be part of the pRS neuron population as they clearly comprised a separate, distinct group. The contralateral pRS neuron population at this level maintained a more restricted location in the ventrolateral corner of the PnO, with some neurons located just outside the putative ventrolateral border and spreading into the ventral nucleus of the lateral lemniscus (VLL).

Moving further caudally into the PnC (Figure 2C), the ipsilateral pRS population shifted ventrally and medially, and was more clearly separated from the labeled neurons in the dorsal part of the SubCA. Contralateral pRS neurons at this level were substantially less numerous and more faintly labeled.

At the most caudal level (Figure 2D), the ipsilateral pRS neuron population remained within the putative border of the PnC but shifted slightly medially. The contralateral pRS population on the other hand shifted laterally outside of the putative PnC border into the region containing the superior olive (SO) and the intermediate reticular nucleus (IRt). Because the neurons involved maintained contiguity with the contralateral pRS population at more rostral levels and did not generate or associate with a separate group of labeled neurons (see 3D reconstructions below), we consider them to be part of the contralateral pRS population.

We defined operationally the border between pons and medulla, which inherently delineates the caudal limit of the pRS neuron population, as the level where labeled raphespinal neurons appeared (neurons in raphe pallidus (RPa) in Figure 2D).

Detailed topography of the ipsilaterally and contralaterally projecting pRS neurons

The topography of the ipsilateral and contralateral pRS neuron subpopulations and their spatial relationship was quantified in the two parasagitally-sectioned preparations that were used for spatial distribution plots.

The plot in Figure 3A shows the mediolateral positions of ipsilateral (magenta circles) and contralateral (green circles) pRS neurons along the rostrocaudal axis, in effect presenting a ventral view of the pRS neuron population. The two subpopulations have been placed on the same side to illustrate the degree of overlap and segregation. However, a plot of the non-overlapped distributions can be found in Supplementary Figure 1A. As shown, the ipsilateral pRS neuron subpopulation occupied a more medial position than its contralateral counterpart, at all rostrocaudal levels. This view also shows that in the ipsilateral subpopulation a distinct mediolateral shift occurred midway along the rostrocaudal axis (at about 400 μm from the caudal limit of the PRF). The average distance from the midline of the pRS neurons located above and below this shift differed by 165 μm.

The plot in Figure 3B shows the dorsoventral positions of ipsilateral and contralateral pRS neurons along the rostrocaudal axis, in effect presenting a side view of the pRS neuron population. This view shows clearly the more dorsal position of the ipsilateral pRS neuron subpopulation relative to its contralateral counterpart, as well as the gradual dorsal to ventral shift of each population moving from rostral to caudal. This dorsal to ventral shift results from the gradual curvature of the pRS neuron population as it follows the natural curvature of the longitudinal axis of the pons.

The plot in Figure 3C shows the mediolateral positions of ipsilateral and contralateral pRS neurons along the dorsoventral axis, in effect presenting an axial view of the pRS neuron population. This view shows a relatively sharp segregation between the ipsilateral and contralateral pRS populations, which was not as evident in Figure 3A or B because the line of segregation is angled with respect to both the frontal and the sagittal planes. This view also shows that each population is sharply delineated eccentrically to the line of segregation, mediodorsally and lateroventrally for the ipsilateral and contralateral pRS populations, respectively.

Altogether the data indicate that, despite a partially overlapping spatial distribution in the PnO and PnC regions, the ipsilateral and contralateral pRS neurons have characteristic locations with the ipsilateral subpopulation occupying a more medial and dorsal position.

Estimates of pRS neuron numbers

To estimate the number of ipsilateral and contralateral pRS neurons, we used two approaches. In the first approach, we counted the pRS neuron soma outlines drawn in the position plots from the two preparations used for Figure 3. The estimates obtained with this method indicate that the numbers of pRS neurons were clearly larger on the ipsilateral side than on the contralateral side throughout the rostrocaudal extent of the pons (Figure 3D). In the second approach, we counted the individually marked pRS neurons in the three 3D-reconstructed brainstems that had received tracer application in the VF+LF (thus labeling the entire pRS neuron population) and multiplied by a factor of 6 (see Material and Methods). In these preparations, for which we had no cytoarchitectonic information, we made a tentative division into PnO and PnC domains at the mediolateral discontinuity in the ipsilateral pRS neuron population described in the previous section (Figure 3A). Estimates were obtained separately for pRS neurons in the PnO and PnC (Table 2), showing that the ipsilateral population was roughly equally divided between the PnO and PnC (376 versus 352 neurons) whereas the contralateral population was clearly more concentrated in the PnO than in the PnC (184 versus 28 neurons). Hence, although ipsilateral pRS neurons were more numerous than contralateral pRS neurons at all rostrocaudal levels, the ipsilateral predominance was much more obvious caudally within the region corresponding to the PnC.

Descending pRS axons entered the spinal cord along a broad mediolateral swath of white matter. To examine the possibility of an internal organization of the pRS neurons related to axon trajectories within the white matter, in nine preparations we restricted labeling to one of three roughly equal zones of the combined VF+LF (Zones 1-3; Figure 1 and cartoons at the bottom of Figure 4). The three preparations shown in Figure 4 were cut transversely at 50 μm and were used for imaging purposes only. The remaining six preparations were reconstructed and used for estimating the relative number of pRS neurons projecting in Zones 1-3 (Table 2, Figure 5). Zones 1-3 were not intended to match any traditional subdivisions of the white matter, but our assessment indicates that Zone 1 contains only VF fibers, Zone 3 contains mostly LF fibers, and Zone 2 contains parts of both, but probably more VF than LF.

Tracing selectively from each zone resulted in distinct, reproducible patterns of labeling within the pRS neuron populations (Table 2, Figures 4, 5). Zone 1 (column A in Figure 4) labeled many ipsilateral but few contralateral pRS neurons, Zone 2 (column B in Figure 4) labeled ipsilateral and contralateral pRS neurons in proportions similar to their numbers in VF+LF preparations, whereas Zone 3 (column C in Figure 4) labeled few ipsilateral but many contralateral pRS neurons. The zone-related distribution of ipsilateral pRS neurons showed a clear differentiation along the rostrocaudal axis. Zone 1 labeled relatively more ipsilateral pRS neurons in the PnC than the PnO (more evident in Table 2 than in Figure 4), Zone 2 labeled them about equally in the PnO and PnC (roughly in proportion to their numbers in VF+LF-labeled preparations), whereas Zone 3 labeled hardly any ipsilateral pRS neurons in the PnC. There was less rostrocaudal differentiation of contralateral pRS neuron labeling as a function of zone, except that Zone 1 only very rarely labeled any contralateral pRS neurons within their most prevalent location in the ventrolateral region of the PnO. These relationships can also be appreciated in the 3D reconstructions shown in Figure 5.

We note that in Table 2, the numbers of pRS neurons labeled from the different zones do not add up to the numbers obtained when labeling the VF+LF in its entirety. The most likely explanation is that the cuts made to label the different zones overlapped slightly from preparation to preparation, and where axon density is high (for example at the transition from Zone 1 to Zone 2), even minor overlap could lead to labeling of large numbers of “unintended” axons. Thus, we do not emphasize the neuron numbers here, but rather focus on the very clear correlation between topography within the pRS neuron populations and mediolateral location of the descending axons.

To summarize, the number of ipsilateral pRS neurons reaches on average about 3 times the number of contralateral pRS neurons and this relative predominance is particularly apparent in the PnC. The majority of ipsilateral pRS neurons in the PnO and PnC was labeled from the medial part of the VF (Zone 1) but a substantial number was labeled from the lateral part of the VF (Zone 2). In contrast, the majority of contralateral pRS neurons in both PnO and PnC was labeled from the LF (Zone 3).

Regional differences in pRS neuron soma size

Examination of labeled ipsilaterally- and contralaterally-projecting pRS neurons in low magnification parasagittal sections (Figure 6A and 6B, respectively) suggests the presence of regional differences in soma sizes in each population. As shown in Figure 6C-E, measurements of soma size demonstrated differential distributions along the different axes. In the PnO (defined as above the dotted line in Figure 6A and 6B), average soma size was similar in the two pRS neuron populations (grand averages: ipsilateral: 178.7 ± 81.7 μm^2; contralateral: 181.3 ± 67.6 μm^2) and relatively constant along the rostrocaudal axis (Figure 6C). By contrast, in the PnC (below the dotted line in Figure 6A and 6B), average soma size was noticeably larger in the ipsilateral population (accompanied by increased variability; 235.0 ± 102.2 μm^2) and smaller in the contralateral population (150.5 ± 49.8 μm^2). Along the mediolateral axis (Figure 6D), average soma size varied less. Finally, along the dorsoventral axis (Figure 6E) there was a clear tendency for increasing soma size in the ipsilateral population moving from dorsal to ventral, while there was no clear trend in the contralateral population.

PRS neuron density

Given the regional differences in soma size along the rostrocaudal axis, we decided to assess whether pRS neuron density also differed along this axis (Figure 7). Neuron density was obtained directly from the position plots shown in Figure 3 and averaged in the transverse plane (thick vertical bars in graph of Figure 7). For both the ipsilateral and contralateral pRS populations, the density was clearly lowest in the most rostral reaches of the PnO, while for the remainder of the PnO and for the PnC it was variable without any clear tendency along the rostrocaudal axis. The variable density suggested that there might exist differences in the intercalation of pRS neurons with other neuron populations or with neuropil. To assess the former possibility, we labeled the pRS neurons in the GAD67-GFP and the GIN transgenic mouse strains in which putative GABAergic neurons express GFP (Figure 8). In the GAD67-GFP mouse, numerous putative GABAergic interneurons were found in the PnO and PnC and these were interspersed among the ipsilateral and contralateral pRS neurons. In the GIN mouse, putative GABAergic interneurons were found nearly exclusively in the PnC, distributed primarily among ipsilateral pRS neurons due to the paucity of contralateral pRS neurons in the PnC. Thus, these two different subpopulations of putative GABAergic neurons were differentially distributed among pRS neurons in the PnO and PnC.

Trajectories of pRS axons in the brainstem

Retrograde labeling with conjugated dextrans also reveals information about the trajectories of the labeled pRS axons. As shown in the examples illustrated in Figure 8, we sectioned a set of labeled

preparations in specific planes designed to align with pRS axon trajectories. These planes were deduced from the material we had sectioned in the transverse, horizontal and sagittal planes.

As a rule, the axons of the ipsilateral pRS neurons (Figure 9A-D) projected initially in a mediodorsal direction and followed quite strictly the natural transverse plane of the pons (the plane changes gradually along the rostrocaudal axis in keeping with the curvature of the pons). As they approached the MLF, ipsilateral pRS axons made a sharp, approximately 90-degree turn towards the spinal cord (arrowheads in Figure 9B-D) and formed a loosely organized axon bundle, the densest part of which adjoined the MLF. In confocal stacks from different parasagittal or transverse planes through the PnO (Figure 9B) or the PnC (Figure 9A, C-D), it can be appreciated that before turning to descend, many ipsilateral pRS axons coursed all the way to their most medial position while maintaining the same rostrocaudal level (best illustrated by the color-code for depth in Figure 9C,D).

The axons of the contralateral pRS neurons located in the PnO had a trajectory similar to that of the ipsilateral pRS axons but with some notable differences. They initially projected in a dorsomedial direction and upon reaching a specific dorsal point, turned abruptly towards the midline (Figure 9E). After they crossed the midline, they joined a forest of labeled axons in this area. Presumably they here turn in a caudal direction but the density of labeled axons prevented us from following individual axons. The entire axonal trajectory of the contralateral pRS axons has been captured in Figure 9E with at least one axon visible throughout the trajectory up to the caudal turn. The trajectory can also be appreciated in Figure 2C and Figure 7C, despite the fact that the section planes used here were not adapted to show it in its entirety. The few contralateral pRS axons originating in the PnC were too weakly labeled to follow with certainty.

Discussion

General overview of results

Through selective retrograde labeling, we have characterized the internal organization of the pRS neuron population, with particular emphasis on the spatial relationship between the ipsilaterally and contralaterally projecting subpopulations and on the topographical relationship to axon trajectories and funicular distributions. We note that several internal features exhibit a marked discontinuity at about 450µm from the caudal limit of the PRF, which we propose marks the transition from PnO to PnC. In the summary that follows we use the terms PnO and PnC for respectively the rostral and caudal parts of the PRF defined by this discontinuity, but we emphasize that the division has not yet been fully validated by direct cytoarchitectonic identification in retrogradely labeled preparations (see, for example, Diaz et al., 2003). Our salient findings are: 1) ipsilateral pRS neurons are 3-fold more numerous than contralateral pRS neurons; 2) ipsilateral pRS neurons are equally divided between the PnO and PnC, whereas contralateral pRS neurons are most prevalent within the PnO; 3) ipsilateral and contralateral pRS neuron populations are spatially segregated; 4) ipsilateral and contralateral pRS neurons exhibit opposite rostrocaudal gradients in soma size; 5) pRS neuron density varies, suggesting that filling of space between pRS neurons by neuropil and other intercalated neuron populations also varies; 6) two different subtypes of putative GABAergic interneurons are differentially distributed among the pRS neurons; 7) ipsilateral and contralateral pRS neurons have distinct axon trajectories within the brainstem; 8) ipsilateral and contralateral pRS axons target the ventral and lateral spinal white matter differentially and in opposing gradients, such that ipsilateral pRS axons enter predominantly the medial region (VF and ventral part of LF) and contralateral pRS axons enter predominantly the lateral region (dorsal part of LF). Additional targeting is seen within the ipsilateral pRS axon population, with ipsilateral axons originating from the PnC and the PnO coursing respectively medially and laterally within their overall gradient. A summary of the principal features of organization and axon trajectory are summarized in Figure 10.

Technical considerations

Determining pRS neuron distribution and number with retrograde labeling

Identifying neurons in the PRF as pRS neurons requires demonstrating that they project to the spinal cord. Retrograde labeling, as done here, is a practical way to ensure this. There are limitations to retrograde labeling techniques that can affect the assessment of neuron distribution and number, however. Earlier studies have shown that despite providing dependable and reproducible patterns of labeling in the central and peripheral nervous system, retrograde labeling with conjugated dextrans typically is not 100% efficient and therefore underestimates the total number of neurons within a given labeled population (see for example Stokke et al., 2002, who demonstrated suboptimal retrograde

labeling of spinal interneurons). Moreover, neuron counts obtained from sections are subject to potential counting errors, which can either overestimate or underestimate neuron number, depending on circumstances (Abercrombie, 1946; Hendry, 1976; Williams and Rakic, 1988). This can be overcome to a large extent by stereological methods (Gundersen et al., 1988; Williams and Rakic, 1988; West, 1993), which we did not employ. At least one report, from the lamprey, indicates that retrograde labeling of reticulospinal neurons with conjugated dextrans may be biased towards larger axon caliber (Brodin et al., 1988). Labeling bias of this type is important, since insufficient or absent labeling of a projection neuron subpopulation would clearly misrepresent the real picture. Of relevance in this regard is our observation that the more caudal contralateral pRS neurons were consistently labeled with weaker intensity than other pRS neurons. We have ruled out that this weak labeling is artifactual through an extensive series of control experiments to test for indirect contamination from the application site to axons not intended to be labeled (not shown), and since these neurons are among the closest to the application site it seems unlikely that axon length is a decisive factor. We have therefore no good explanation for why the labeling was consistently weaker in this particular pRS neuron subpopulation.

On this backdrop we cannot guarantee that the picture we provide is complete, but given the consistency of labeling pattern we can safely conclude that the pRS neuron population consists of at least a larger ipsilateral subpopulation and a smaller contralateral subpopulation. Moreover, quantitation errors due to sectioning would not be expected to affect the two subpopulations differently, so we are also confident in our description of their regional segregation and relative numbers. Obviously, the variability in pRS neuron number estimates we report here could be either technical (labeling efficiency, labeling bias, counting) or biological, or any combination of these. Thus, we do not consider these numbers to be more than estimates. Taken at face value, these estimates indicate that there are about 900 pRS neurons in total on each side of the PRF of which about a fourth are contralaterally projecting. It should be noted that Liang et al (2011) report substantially more pRS neurons in the adult mouse, on the order of 6,500 on each side, using Fluorogold as tracer and 96 hours of in vivo tracer transport time. They also caution that their counts of retrogradely labeled neurons should be considered only as estimates. They, like us, did not use stereological methods or counting correction factors. It remains to be determined what the discrepancy between neonatal and adult counts represents.

The vagaries of cytoarchitectonics

As we have pointed out in earlier studies of bulbospinal neuron populations in which we have compared retrogradely labeled neuron populations to cytoarchitectonic divisions of the hindbrain (Díaz et al 2003), the mapping of cytoarchitectonic boundaries is by nature subjective and can vary

from investigator to investigator and even from study to study by the same investigator, especially if different section planes are used. Thus, we feel that cytoarchitectonic boundaries should be used with great caution. Here, we have transferred boundaries of the PnO and PnC, and of other structures in their vicinity, from the atlas generated by Paxinos et al. (2007), aligning them with landmarks visible in our material. Since we have not used Nissl staining as in that atlas, but rather methylene blue staining which provides less cytoarchitectonic detail, and because methylene blue stained sections were intercalated between sections stained for the conjugated dextran tracers, the alignment further depends on subjective interpretation. Given these caveats, we find that coherent clusters of pRS neurons are located largely but not completely within the putative boundaries of the PnO and PnC. We suggest that boundary transgressions, to the extent that they do not obviously encroach on other well-defined neuron clusters nearby, are of minimal functional significance. It seems most likely that anatomical coherence of retrogradely labeled neuron populations is a direct result of early patterning mechanisms that define axon projection pathway and to some extent synaptic connectivity (see Diaz et al., 2003, for discussion), such that this coherence should be considered a stronger indication of common identity than should compliance to subjectively defined boundaries.

Definition of axon trajectories and funicular destinations

We have described pRS axon trajectories within the brainstem based on the behavior of those axons that are most easily visualized within standard section planes. Although in some instances we have employed atypical section planes to better capture some of these trajectories, we cannot claim that all pRS axons behave as described. Our description is likely to be generally applicable, but there may be exceptions. A fully 3D in situ analysis using newly available tissue clearing methods and large volume confocal reconstruction approaches could provide a more certain assessment.

We have used selective tracer application to describe the spinal funicular destinations of the pRS axons. This analysis shows a clearly differential targeting both between and within the ipsilateral and contralateral pRS neuron subpopulations. The three application sites were generated manually and in separate preparations, however, and some overlap between them is therefore unavoidable. Indeed, the estimated numbers of pRS neurons projecting into each zone do not sum to the total estimate, a certain indication of overlap. We therefore do not place undue emphasis on these numbers, preferring to use the results as a coarse indication of the pattern of axon targeting, which in our view suggests mutually opposing gradients rather than distinct white matter tracts.

Our Zone 3 tracer application extended beyond the dorsal limit of the LF, to ensure that axons throughout the full extent of the LF were retrogradely labeled. With anti-neurofilament staining, we could discern a thin shell of axons, also visible in methylene blue stained sections, beyond the

presumed dorsal limit of the LF (see Figure 1B,C). This has been identified as the dorsolateral funiculus (DLF, or Lissauer's tract), since it lies dorsal to the lateral cervical nucleus (Sengul et al., 2012). Thus, we are confident that our tracer applications have engaged all of the LF and thus the entire dorsoventral extent of the white matter region that contains bulbospinal axons in the neonate. However, the LF becomes larger and may extend further dorsally with continued postnatal development due to the addition of late developing, spinally projecting axon populations, such as corticospinal axons. It is not known whether these later arriving axons include additional pRS axons.

Internal organization of the pRS neuron population

Comparison to other retrograde tracing studies in the mouse and rat

Several previous retrograde tracing studies have demonstrated projections from the PRF to the spinal cord in the mouse and rat, ranging from embryonic to adult stages (mouse: Auclair et al., 1999; Vanderhorst and Ulfhake, 2006; Liang et al., 2011, 2015; rat: Basbaum and Fields, 1979; Satoh 1979; Watkins et al 1980, 1981; Leong et al., 1984a,b; Newman, 1985; Jones and Yang, 1985; Nudo and Masterton, 1988; Rye et al 1988; Shen et al 1990; Masson et al 1991; Lakke, 1997; Auclair et al., 1999; Reiner et al 2008; Huma et al 2014). Only three of these studies combined unilateral tracer application with contralateral spinal cord hemisection to ensure unilateral tracing so that the laterality of projections could be unequivocally documented (Basbaum and Fields 1979; Auclair et al., 1999; Vanderhorst and Ulfhake, 2006), as we have done here. In eight other studies, in the adult mouse or rat, unilateral applications were made but not combined with contralateral lesions to ensure unilateral tracing (Watkins et al 1980, 1981; Newman 1985; Nudo and Masterton, 1988: Liang et al., 2011, 2015; Reiner et al 2008; Huma et al 2014). These studies will receive additional attention below. In the remaining studies the laterality of retrograde tracing is inherently questionable.

Nearly all of the above studies have shown that both the PnC and the PnO project to the spinal cord; a few describe projections only from the PnC. Liang et al. (2011) also distinguish the PnV (ventral pontine reticular nucleus), containing a minor population of reticulospinal neurons, which may in fact be the most rostral part of the medullary gigantocellular nucleus, potentially misconstrued as having a pontine location because of mismatch between coronal sections of the adult brain and the planes of rhombomere boundaries (see below). Regarding laterality, Basbaum and Fields (1979), Auclair et al (1999), Vanderhorst and Ulfhake (2006) and Huma et al (2014) all report an ipsilateral predominance in the projection of pRS neurons throughout the PRF, including both the PnO and the PnC. Newman (1985) concurs, with a distinction between the PnC (his RPoC) pars alpha and beta, which project respectively with contralateral and ipsilateral predominance, and between the PnO (his RPoO) medialis and lateralis, which project respectively with a weak ipsilateral predominance and no lateral bias. Since RPoC pars beta and RpoO medialis correspond to the more dorsal and medial regions of

the PnC and PnO, respectively, the ipsilateral predominance of pRS neurons in these specific regions reported by Newman (1985) correlates well with our results, as does the contralateral predominance of pRS neurons in the RPoC pars alpha. Nudo and Masterton (1988) also show a marked ipsilateral predominance in the pRS projection, but only illustrate one level in the PRF, evidently from the PnC. Watkins et al (1980) report an ipsilateral predominance, but since their tracer applications were targeted to the DLF with the aim of retorgradely labeling the raphespinal projection, only relatively few pRS neurons were labeled, in the most ventral region of the PRF. Using the same DLF-targeted tracer applications, Watkins et al (1981) report bilateral labeling in PnC and contralateral labeling in PnO, again with only few pRS neurons labeled. In contrast to these studies, Reiner et al (2008) report equal numbers of ipsilateral and contralateral pRS neurons irrespective of whether injections were made at cervical, thoracic or lumbar levels, and Liang et al. (2011) report a substantial contralateral predominance of projections from the PnO following tracer injections into the cervical spinal cord, although they do report an ipsilateral predominance for the PnC. Liang et al (2015) present images that suggest an *ipsilateral* predominance in the PnO following tracer injections in the *lumbar* spinal cord. Since a large proportion of pRS neurons in the PnO project very medially (in the ipsilateral Zone 1), it seems plausible that the contralateral predominance of the PnO projection reported by Liang et al. (2011) following cervical tracer injections and the nearly symmetrical laterality reported by Reiner et al (2008) may have arisen from contamination of medially located axons on the side contralateral to the injection. This would label ipsilaterally projecting pRS neurons in the PnO contralateral to the tracer injection site, which would then be misinterpreted as contralaterally projecting. An additional sign of such potential contamination is the much more symmetrical labeling of neurons in the ventral portion of the nucleus subcoeruleus reported by Liang et al. (2011) than is reported by Vanderhorst and Ulfhake (2006) and here. The discrepancies in laterality underscore the importance of using lesions in conjunction with tracer injections if the aim of retrograde labeling is to determine the laterality of axon descent, avoiding the complicating issues of contralateral tracer contamination and commissural collateralization of axons within the spinal cord.

Huma et al. (2014) also aimed to assess, in the adult rat, the white matter trajectories of bulbospinal neurons, including those in the PRF. They combine unilateral lumbar injection of one retrograde tracer with ipsilateral injection of another retrograde tracer in either the MLF or the caudal ventrolateral medulla. They find a predominantly medial targeting of ipsilateral pRS axons originating from both the PnO and the PnC and a predominantly lateral targeting of contralateral pRS axons originating from the PnC, similar to what we report in the neonate. However, they report that contralateral pRS neurons in the PnO project predominantly medially, which does not fit with our results. Since they did not ensure unilateral labeling with a contralateral lesion, there again is a possibility that this discrepancy arises from contamination of the MLF on the side opposite the injection.

Comparison to retrograde tracing studies in other mammals

Although an exhaustive description of the literature on bulbospinal projections in non-rodent mammals is beyond the scope of this discussion, it is worth noting that the pRS projection has been described in a variety of mammalian species, particularly the opposum (Martin et al. 1979; Cabana and Martin 1984; Martin et al. 1988), cat (Nyberg-Hansen 1965; Petras 1967; Basbaum and Fields 1979; Tohyama et al. 1979; Holstege et al. 1979; Hayes and Rustioni 1981; Mitani et al 1988; Rice et al 2010) and non-human primates (Carlton et al 1985; Sakai et al 2009). In general, these studies indicate that asymmetry with ipsilateral predominance of the pRS projection is a conserved feature, although discrepancies regarding laterality also exist in this literature.

Relationship to developmental patterning

By comparison to our earlier study of reticulospinal and vestibulospinal neurons in the mouse and rat embryos, it seems quite clear that the pRS neurons are located in the rostrocaudal domain that derives from rhombomeres (r) 1-4 (Auclair et al., 1999). In that earlier study, we also noted the development of a distinct discontinuity in the shape of the ipsilateral and contralateral pRS neuron populations, located at the transition from r2 to r3. Thus, we propose that this discontinuity in embryos corresponds to the discontinuity reported here that we have operationally defined as the boundary between PnO and PnC. This would mean that the PnO derives from r1-2 and the PnC derives from r3-4. This rhombomere-related discontinuity becomes apparent about a day after pRS axons reach the spinal cord (Auclair et al., 1999), indicating that it originates through cell aggregation imposed on initially more evenly distributed neurons – in other words a relatively late feature of patterning. By contrast, a differential location of ipsilateral and contralateral pRS neuron subpopulations in the transverse plane is evident as early as the pRS neurons can be retrogradely labeled from the spinal cord (Auclair et al., 1999), suggesting that this feature of patterning originates early, likely because the two subpopulations originate from different dorsoventral progenitor domains.

Relationship to function

The numerical predominance of ipsilateral versus contralateral pRS neurons is significant relative to our previous report on the synaptic inputs from pRS neurons to spinal MNs (Sivertsen et al., 2014). In that study we found both an ipsilateral and a contralateral projection from the PRF to MNs, but the ipsilateral projection transmitted more faithfully and appeared to be more direct. Accordingly, we suggest that this difference in functional connectivity is due at least in part to differences in the spinal targets of the ipsilateral and contralateral pRS neurons. Ipsilateral pRS neurons evidently innervate

MNs either directly or through few intermediate INs, whereas contralateral pRS neurons innervate primarily INs. How this relates to behavior is not yet clear. The PnC is involved in postural control and is a main relay for auditory stimulus-elicited startle reactions (Davis et al 1982; Femano et al 1984; Yeomans and Frankland 1996). The latter generates widespread and bilateral activation of head, neck, trunk and limb musculature, whereas the former can involve more selective activation of muscles. The PnO has been implicated in the induction of widespread muscle atonia in connection with REM sleep and also overlaps the mesopontine tegmental anesthesia area, which when pharmacologically activated exerts widespread spinal anesthesia and atonia (Reiner et al 2008). Anterograde tracing in several mammalian species including the mouse have shown that axons from PnO and PnC terminate throughout the length of the spinal cord and differential retrograde tracing from multiple spinal levels suggests a high degree of rostrocaudal collateralization by individual pRS axons (selected studies in rodents: Sirkin and Feng, 1987; Reiner et al 2008; Liang et al; 2015). As in the cat (Matsuyama et al 1993, 1999), pRS axon terminals in rodents are particularly focused on the ipsilateral laminae VII and VIII, which are known to contain premotor interneurons, and are also found in the contralateral cord. Given the difficulty of distinguishing terminals derived from individual axons and the diversity of spinal interneurons that populate the regions of termination, a more comprehensive functional characterization of the spinal targets of the PnO and PnC and their ipsilateral and contralateral pRS subpopulations is warranted.

Differences in pRS soma size can be related to several functional characteristics, including packing density of synaptic input, input resistance and its effects on synaptic integration, susceptibility to electrical stimulation, thickness and conduction velocity of axons, and number of axon terminal branches and synaptic contacts on target neurons. Thus, it is likely that the regional differences we observe in soma size reflect functional heterogeneity within the pRS population.

Neuron density determines how much space surrounds each neuron and bears a direct relationship to neuropilar density and the potential for positing intercalated neurons. Since not all projection neurons in the PRF project to the spinal cord (Jones and Yang, 1985; Lingenhohl and Friauf, 1994), it is likely that submaximal neuron densities within the pRS neuron subpopulations relate to the presence of additional PRF projection neuron populations that project elsewhere or the presence of local interneurons, such as the putative GABAergic interneurons that we show are intercalated among the pRS neurons.

Topography of axon trajectories including their funicular projections

The trajectories of pRS axons within the brainstem and their funicular targeting in the spinal white matter clearly differ between the ipsilateral and contralateral pRS neuron subpopulations. Ipsilaterally-projecting pRS axons course dorsally towards the midline, parallel to each other in a broad swath

matching the rostrocaudal extent of their parent somata, before turning to descend in a largely medial location that overlaps but is not restricted to the MLF. The overall trajectory is very similar to that described for individual pRS neurons in the PnC in the adult rat (Lingenhohl and Friauf, 1994). By contrast, contralaterally projecting pRS axons follow a more tortuous path to their descending turning point, starting in a dorsomedial direction and then veering ventrally before crossing the midline. They cross the midline in a rostrocaudally narrower bundle relative to the ipsilaterally projecting axons. Upon turning to descend, the ipsilaterally and contralaterally projecting axons tend to take up more medial and lateral positions, respectively, and as they reach the spinal cord, they distribute with opposite gradients within the VF and LF. These distinct routes imply differences in the pathfinding cues that the ipsilaterally and contralaterally projecting axons follow as they navigate towards the spinal cord.

Differences in funicular trajectories within the spinal cord have a clear functional significance, as they dictate proximity to specific laminae and to the dendrites of potential target neurons. Thus, we would expect that the more medial trajectories of the ipsilaterally projecting pRS axons would especially facilitate connections with spinal neurons in the ventromedial parts of the grey matter, including axial MNs and INs in lamina VIII and the medial part of lamina VII, whereas the more lateral trajectories of the contralaterally projecting neurons would bring them closer to limb-innervating MNs, sympathetic preganglionic neurons and INs in the lateral parts of lamina VII and lamina VI. The reach of target neuron dendrites complicates this picture of course, underscoring the importance of physiological confirmation of connectivity.

Our description also provides a tool that can facilitate the physiological assessment of synaptic connections between the pRS neurons and spinal neuron targets, by indicating where lesions can be placed to restrict impulse traffic to identifiable axon subpopulations. For example, by making a midline lesion in the pons together with a lesion in the upper cervical cord sparing Zone 1, transmission of impulses elicited by stimulation of the PRF would be biased towards ipsilateral pRS neurons in the PnC, whereas an upper cervical lesion sparing Zone 3 would bias towards ipsilateral pRS neurons in the PnO.

Future directions

We are currently pursuing two lines of research to further characterize the pRS neurons. The first of these involves neurotransmitter phenotyping. In our study of synaptic connections from pRS neurons onto spinal MNs, we used calcium imaging that readily reveals excitatory connections (Sivertsen eal., 2014). However, there is evidence that activation of spinal MNs by electrical stimulation within the ipsilateral PnC can be inhibited by concomitant stimulation within the contralateral PnC (Femano et al 1984). Thus, we are performing a variety of assays to establish the neurotransmitters used by the

ipsilateral and contralateral pRS neuron subpopulations. The second line of research is focused on developmental patterning. Since the ipsilateral and contralateral pRS neuron subpopulations appear to derive from different dorsoventral domains in the developing hindbrain, we are carrying out fate mapping experiments to determine their transcription factor-defined progenitor domains of origin. This will provide information about how the two subpopulations become specified to differentiate their specific characteristics, as well as an avenue for transgenic manipulation, including the use of optogenetic tools for more selective physiological studies.

Acknowledgements

We thank Kobra Sultani for technical assistance with the mouse colony and Sveinung Lillehaug for help with Neurolucida reconstructions.

Conflicts of interest

The authors declare no conflicts of interest associated with this work.

Author contributions

All authors had full access to all the data in the study and take responsibility for the integrity of the data and the accuracy of the data analysis. Study concept and design: MSS, MCP, JCG. Acquisition of data: MSS, JCG. Analysis and interpretation of data: MSS, MCP, JCG. Drafting of the manuscript: MSS, JCG. Critical revision of the manuscript for important intellectual content: MSS, MCP, JCG. Approval of final manuscript draft: MSS, MCP, JCG. Statistical analysis: MSS, JCG. Obtained funding: MCP, JCG. Administrative, technical, and material support: JCG. Study supervision: JCG.

List of abbreviations

4V	Fourth ventricle	Pn	Pontine nuclei
5N	Motor trigeminal nucleus	PnC	Pontine reticular nucleus, caudal part
5TT	Motor trigeminal nucleus, tensor tympani part	PnO	Pontine reticular nucleus, oral part
6N	Abducens nucleus	Pr5	Principal sensory trigeminal nucleus
Bar	Barrington's nucleus	pRS	Pontine reticulospinal
DC	Dorsal cochlear nucleus	RIP	Raphe interpositus nucleus
DMTg	Dorsomedial tegmental area	Rpa	Raphe pallidus nucleus
DRC	Dorsal raphe nucleus, caudal part	rs	Rubrospinal tract
DTgP	Dorsal tegmental nucleus, pericentral part	RtTg	Reticulotegmental nucleus of the pons
IRt	Intermediate reticular nucleus	SO	Superior olive
KF	Kölliker-Fuse nucleus	SpVe	Spinal vestibular nucleus
LC	Locus coeruleus	Su5	Supratrigeminal nucleus
LDTg	Laterodorsal tegmental nucleus	SubCA	Subcoeruleus nucleus, alpha part
LVe	Lateral vestibular nucleus	SubCD	Subcoeruleus nucleus, dorsal part
mlf	Medial longitudinal fascicle	SuVe	Superior vestibular nucleus
MnR	Median raphe nucleus	Tz	Trapezoid body
MVeMC	Medial vestibular nucleus, magnocellular part	VeCb	Vestibulocerebellar nucleus
MVePC	Medial vestibular nucleus, parvicellular part	VLL	Ventral nucleus of the lateral lemniscus
PCRtA	Parvicellular reticular nucleus, alpha part	Vtg	Ventral tegmental nucleus
PMnR	Paramedian raphe nucleus	X	Nucleus X

Literature Cited

Abercrombie M. 1946. Estimation of nuclear population from microtome sections. Anat Rec 94:239-47.

Auclair F, Marchand R, Glover JC. 1999. Regional patterning of reticulospinal and vestibulospinal neurons in the hindbrain of mouse and rat embryos. J Comp Neurol 411(2):288-300.

Baker SN. 2011. The primate reticulospinal tract, hand function and functional recovery. J Physiol 589:5603-12.

Basbaum AI, Fields HL. 1979. The origin of descending pathways in the dorsolateral funiculus of the spinal cord of the cat and rat: further studies on the anatomy of pain modulation. J. Comp. Neurol. 187:513–531.

Brodin L, Grillner S, Dubuc R, Ohta Y, Kasicki S, Hokfelt T. 1988. Reticulospinal neurons in lamprey: transmitters, synaptic interactions and their role during locomotion. Arch Ital Biol 126(4):317-45.

Cabana T, Martin GF. 1984. Developmental sequence in the origin of descending spinal pathways. Studies using retrograde transport techniques in the North American opossum (Didelphis virginiana). Brain Res. 317:247-63.

Carlton SM, Chung JM, Leonard RB, Willis WD. 1985. Funicular trajectories of brainstem neurons projecting to the lumbar spinal cord in the monkey (Macaca fascicularis): a retrograde labeling study, J. Comp. Neurol. 241:382–404.

Cepeda-Nieto AC, Pfaff SL, Varela-Echavarria A. 2005. Homeodomain transcription factors in the development of subsets of hindbrain reticulospinal neurons. Mol Cell Neurosci 28(1):30-41.

Davis M, Gendelman DS, Tischler MD, Gendelman PM. 1982. A primary acoustic startle circuit: lesion and stimulation studies. J Neurosci. 2:791-805.

Diaz C, Glover JC, Puelles L, Bjaalie JG. 2003. The relationship between hodological and cytoarchitectonic organization in the vestibular complex of the 11-day chicken embryo. J Comp Neurol 457(1):87-105.

Drew T, Prentice S, Schepens B. 2004. Cortical and brainstem control of locomotion. Prog Brain Res 143:251-61.

Femano PA, Schwartz-Giblin S, Pfaff DW. 1984. Brain stem reticular influences on lumbar axial muscle activity. I. Effective sites. Am J Physiol. 246:389-95.

Glover JC. 2000. Development of specific connectivity between premotor neurons and motoneurons in the brain stem and spinal cord. Physiol Rev 80(2):615-47.

Glover JC, Petursdottir G, Jansen JK. 1986. Fluorescent dextran-amines used as axonal tracers in the nervous system of the chicken embryo. J Neurosci Methods 18(3):243-54.

Gundersen HJ, Bendtsen TF, Korbo L, Marcussen N, Moller A, Nielsen K, Nyengaard JR, Pakkenberg B, Sorensen FB, Vesterby A, . 1988. Some new, simple and efficient stereological methods and their use in pathological research and diagnosis. APMIS 96(5):379-94.

Hayes NL, Rustioni A. 1981. Descending projections from brainstem and sensorimotor cortex to spinal enlargements in the cat. Single and double retrograde tracer studies. Exp Brain Res. 41:89-107.

Hendry IA. 1976. A method to correct adequately for the change in neuronal size when estimating neuronal numbers after nerve growth factor treatment. J Neurocytol 5(3):337-49.

Holstege G, Kuypers HG, Boer RC. 1979. Anatomical evidence for direct brain stem projections to the somatic motoneuronal cell groups and autonomic preganglionic cell groups in cat spinal cord, Brain Res. 171:329–333.

Holstege G. 1998. The emotional motor system in relation to the supraspinal control of micturition and mating behavior. Behav Brain Res 92(2):103-9.

Huma Z, Du Beau A, Brown C, Maxwell DJ. 2014. Origin and neurochemical properties of bulbospinal neurons projecting to the rat lumbar spinal cord via the medial longitudinal fasciculus and caudal ventrolateral medulla. Front Neural Circuits doi: 10.3389/fncir.2014.00040.

Jones BE, Yang TZ. 1985. The efferent projections from the reticular formation and the locus coeruleus studied by anterograde and retrograde axonal transport in the rat. J Comp Neurol 242(1):56-92.

Lakke EA. 1997. The projections to the spinal cord of the rat during development: a timetable of descent. Adv Anat Embryol Cell Biol 135:I-143.

Lawrence DG, Kuypers HG. 1968. The functional organization of the motor system in the monkey. II. The effects of lesions of the descending brain-stem pathways. Brain 91(1):15-36.

Leong SK, Shieh JY, Wong WC. 1984a. Localizing spinal-cord-projecting neurons in adult albino rats. J Comp Neurol 228(1):1-17.

Leong SK, Shieh JY, Wong WC. 1984b. Localizing spinal-cord-projecting neurons in neonatal and immature albino rats. J Comp Neurol 228(1):18-23.

Liang H, Paxinos G, Watson C. 2011. Projections from the brain to the spinal cord in the mouse. Brain Struct Funct 215(3-4):159-86.

Liang H, Watson C, Paxinos G. 2015. Projections from the oral pontine reticular nucleus to the spinal cord of the mouse. Neuroscience Letters 584:113–118.

Lingenhohl K, Friauf E. 1994. Giant neurons in the rat reticular formation: a sensorimotor interface in the elementary acoustic startle circuit? J Neurosci 14(3 Pt 1):1176-94.

Martin GF, Humbertson Jr. AO, Laxson LC, Panneton WM, Tschismadia I. 1979. Spinal projections from the mesencephalic and pontine reticular formation in the North American Opossum: a study using axonal transport techniques, J. Comp. Neurol. 187:373–399.

Martin GF, Cabana T, Waltzer R. 1988. The origin of projections from the medullary reticular formation to the spinal cord, the diencephalon and the cerebellum at different stages of development in the North American opossum: studies using single and double labeling techniques. Neuroscience. 25:87-96.

Masson RL, Sparkes ML, Ritz LA. 1991. Descending projections to the rat sacrocaudal spinal cord. J. Comp. Neurol. 302:120–130.

Matsuyama K, Kobayashi Y, Takakusaki K, Mori S, Kimura H. 1993. Termination mode and branching patterns of reticuloreticular and reticulospinal fibers of the nucleus reticularis pontis oralis in the cat: an anterograde PHA-L tracing study. Neuroscience Research, 17:9-21.

Matsuyama K, Mori F, Kuze B, Mori S. 1999. Morphology of single pontine reticulospinal axons in the lumbar enlargement of the cat: A study using the anterograde Tracer PHA-L. J. Comp. Neurol. 410:413–430.

Mitani A, Ito K, Mitani Y, McCarley RW. 1988. Descending projections from the gigantocellular tegmental field in the cat: cells of origin and their brainstem and spinal cord trajectories. J Comp Neurol. 268:546-66.

Newman DB. 1985. Distinguishing rat brainstem reticulospinal nuclei by their neuronal morphology. II. Pontine and mesencephalic nuclei. J Hirnforsch 26(4):385-418.

Nudo RJ, Masterton RB. 1988. Descending pathways to the spinal cord: a comparative study of 22 mammals. J Comp Neurol 277(1):53-79.

Nyberg-Hansen N. 1965. Sites and mode of termination of reticulospinal fibers in the cat. An experimental study with silver impregnation methods, J. Comp. Neurol. 124:71–99.

Oliva AA Jr, Jiang M, Lam T, Smith KL, Swann JW. 2000. Novel hippocampal interneuronal subtypes identified using transgenic mice that express green fluorescent protein in GABAergic interneurons. J Neurosci. 20:3354-3368.

Pasqualetti M, Diaz C, Renaud JS, Rijli FM, Glover JC. 2007. Fate-mapping the mammalian hindbrain: segmental origins of vestibular projection neurons assessed using rhombomere-specific Hoxa2 enhancer elements in the mouse embryo. J Neurosci 27(36):9670-81.

Paxinos G, Halliday G, Watson C, Koutcherov Y, Wang H. 2007. Atlas of the Developing Mouse Brain. First ed. Elsevier.

Perreault MC, Glover JC. 2013. Glutamatergic reticulospinal neurons in the mouse: developmental origins, axon projections, and functional connectivity. Ann N Y Acad Sci 1279:80-9.

Petras JM. 1967. Cortical, tectal and tegmental fiber connections in the spinal cord of the cat, Brain Res. 6:275–324.

Reiner K, Sukhotinsky I, Devor M. 2008. Bulbospinal neurons implicated in mesopontine-induced anesthesia are substantially collateralized. J Comp Neurol. 508(3):418-436.

Rice CD, Weber SA, Waggoner AL, Jessell ME, Yates BJ. 2010. Mapping of neural pathways that influence diaphragm activity and project to the lumbar spinal cord in cats. Exp Brain Res. 203:205-11.

Rye DB, Lee HJ, Saper CB, Wainer BH. 1988. Medullary and spinal efferents of the pedunculopontine tegmental nucleus and adjacent mesopontine tegmentum in the rat. J Comp Neurol. 269:315-341.

Sakai ST, Davidson AG, Buford JA. 2009. Reticulospinal neurons in the pontomedullary reticular formation of the monkey (Macaca fascicularis). Neuroscience. 163:1158-70..

Satoh K. 1979. The origin of reticulospinal fibers in the rat: a HRP study. J Hirnforsch. 20:313-22.

Sengul G, Puchalski RB, Watson C. 2012. Cytoarchitecture of the spinal cord of the postnatal (P4) mouse. Anat Rec (Hoboken) 295(5):837-45.

Shen P, Arnold AP, Micevych PE. 1990. Supraspinal projections to the ventro- medial lumbar spinal cord in adult male rats. J. Comp. Neurol. 300:263–272.

Sirkin DW, Feng AS, 1987. Autoradiographic study of descending pathways from the pontine reticular formation and the mesencephalic trigeminal nucleus in the rat. J. Comp. Neurol. 256:483–493.

Sivertsen MS, Glover JC, Perreault MC. 2014. Organization of pontine reticulospinal inputs to motoneurons controlling axial and limb muscles in the neonatal mouse. J Neurophysiol 112(7):1628-43.

Sivertsen MS, Perreault MC, Glover JC. 2013. Characterization of rostral medullary and pontine reticulospinal projections in the late fetal and neonatal mouse. Soc Neurosci Abstr 43:560.03.

Stokke MF, Nissen UV, Glover JC, Kiehn O. 2002. Projection patterns of commissural interneurons in the lumbar spinal cord of the neonatal rat. J Comp Neurol 446(4):349-59.

Tamamaki N, Yanagawa Y, Tomioka R, Miyazaki J-I, Obata K, Kaneko T. 2003. Development of mouse expressing GFP in GABAergic neurons. Neurosci. Res. Suppl. 25:S77.

Tohyama M, Sakai K, Salvert D, Touret M, Jouvet M. 1979. Spinal projections from the lower brain stem in the cat as demonstrated by the horseradish peroxidase technique. I. Origins of the reticulospinal tracts and their funicular trajectories, Brain Res. 173:383–403.

Vanderhorst VG, Ulfhake B. 2006. The organization of the brainstem and spinal cord of the mouse: relationships between monoaminergic, cholinergic, and spinal projection systems. J Chem Neuroanat 31(1):2-36.

Watkins LR, Griffin G, Leichnetz GR, Mayer DJ. 1980. The somatotopic organisation of the nucleus raphe magnus and surrounding brain stem structures as revealed by HRP slow-release gels. Brain Res. 181:1-15.

West MJ. 1993. New stereological methods for counting neurons. Neurobiol Aging 14(4):275-85.

Williams RW, Rakic P. 1988. Three-dimensional counting: an accurate and direct method to estimate numbers of cells in sectioned material. J Comp Neurol 278(3):344-52.

Figure legends

Figure 1. Overview of retrograde labeling targeted to specific white matter zones

A) Wholemount image of a P0 brainstem retrogradely labeled unilaterally at the level of the C2 ventral root. Labeling was restricted to Zone 1 and performed after removal of the contralateral spinal cord. Diffuse fluorescence produced by retrogradely labeled neurons and axons can be discerned in both medulla and pons, most noticeably in the medial half of the ipsilateral medulla. The preparation is illuminated by both epifluorescence and incident white light to reveal tissue contours. B) Neurofilament immunostaining in a transverse section from the upper cervical spinal cord at P0, illustrating the distribution of axons in the white matter. Arrow indicates the dorsolateral funiculus (DLF). Numbers 1-3 indicate the different zones used for selective retrograde labeling. C) Transverse section from the upper cervical spinal cord at P0, stained with methylene blue to show the white matter (light blue regions), with Zones 1-3 (outlined), and the DLF (arrow) indicated. D) Transverse sections at C2 in preparations with labeling restricted to Zone 1 (left) and Zone 3 (right). Arrow in right panel indicates the C2 ventral root. Scale bars: 500µm (A), 200µm (B-D).

Figure 2. Spatial distribution of pRS neurons and other neuron populations in the pons.

Epifluorescence images (50 µm transverse sections, evenly spaced at 250 µm intervals through the pons at P0) showing retrograde labeling in the pons after applying RDA unilaterally (Ipsi) to the entire VF+LF at C2. Cytoarchitectonically defined boundaries of relevant nuclei and structures adapted from the atlas of (Paxinos et al., 2007) have been superimposed (see Methods). Stippled lines indicate boundaries transferred from the Paxinos et al (2007) atlas, which should thus be considered only as approximate, whereas continuous lines indicate boundaries that could be seen in neighboring sections stained with methylene blue. **A)** Rostralmost section, showing ipsilateral pRS neurons in the PnO (open arrow) lying dorsal to the labeled axons of the rubrospinal tract (rs). Contralateral pRS neurons (filled arrow) lie near the lateral edge of the PnO, in the border area between the PnO and the ventral nucleus of the lateral lemniscus (VLL). **B)** At this level (250 um more caudal than A), ipsilateral pRS neurons form a distinct cluster in the lateral half of the PnO, adjoining the more dorsal group of retrogradely labeled neurons in the nucleus subcoeruleus, alpha part (SubCA). Contralateral pRS neurons lie in the ventrolateral corner of the PnO, similar to their location in A. **C)** Ipsilateral pRS neurons are located centrally in the PnC. A few contralateral pRS neurons are also labeled in the lateral part of the PnC. However, they are weakly labeled, and best seen in the inset displaying the same region at twice the magnification and with enhanced brightness and contrast (filled arrows indicate individual neurons). At this level, axons from contralateral pRS are seen traversing the PnC, the SubCD and the dorsomedial tegmental area (DMTg) before crossing the midline (arrowhead). **D)** In the most caudal region of pons, ipsilateral pRS neurons lie centrally within the PnC where they are enmeshed with labeled axons coursing toward the spinal cord. Contralateral pRS neurons are located

near the ventrolateral corner of the PnC, in a region that according to Paxinos et al (2007) corresponds to the superior olive (SO) and the intermediate reticular nucleus (IRt). They are also shown in the inset on the right hand side. At this level, ipsilateral and contralateral vestibulospinal neurons can also be seen clearly. Note that the location of contralateral pRS neurons outside the indicated confines of the PnO is in our view due to a combination of shifts in the locations of boundaries from the illustrated section to the adjacent methylene blue-stained section and ambiguity in the transfer of the boundaries defined by Paxinos et al (2007).

Figure 3. Spatial relationship between the ipsilateral and contralateral pRS neuron populations.
A-C: Plots showing the positions of individual pRS neurons pooled from two preparations in different planes of view (inset cartoons). Magenta and green circles indicate ipsilateral and contralateral pRS neurons, respectively. Note that both pRS neuron populations are plotted on the same side to emphasize the difference in spatial domains. Because the plots are obtained from parasagitally sectioned preparations, for which mediolateral coordinates automatically become discontinuous according to the spacing of the sections (see Supplementary Figure 1), the mediolateral coordinates have been randomized through the section thickness to provide a smoother representation. **A)** Plot of rostrocaudal versus mediolateral position of each labeled pRS neuron (ventral view). The origin is placed at the point where the midline and the medulla/pons transition meet. . **B)** Plot of rostrocaudal versus dorsoventral position of each labeled pRS neuron (side view). The origin is placed at the point where the ventralmost extent of the 4th ventricle and the medulla/pons transition meet. **C)** Plot of dorsoventral versus mediolateral position of each labeled pRS neuron (axial view). The origin is placed at the point where the ventralmost extent of the 4th ventricle and the midline meet. **D)** Histogram of the number of pRS neurons along the rostrocaudal extent of the pons (divided into 50 μm bins). The value in each bin represents the mean of the number of neurons in the two preparations.

Figure 4. Spatial distribution of pRS neurons that project in different white matter zones.
Column A-C show the spatial distribution of pRS neurons in preparations retrogradely labeled from Zone 1 (A1-4), Zone 2 (B1-4) and Zone 3 (C1-4), respectively. Each column includes 4 transverse sections evenly spaced at 250 μm intervals through the pons, at the levels indicated in the inset at top right. **A1-4)** Zone 1 labels preferentially the ipsilateral pRS neuron population, relatively more at caudal than at rostral levels. **B1-4)** Zone 2 labels both the ipsi- and contralateral pRS populations, in a pattern similar to that seen in preparations labeled from the VF+LF (see Figure 2). **C1-4)** Zone 3 labels preferentially the contralateral pRS neuron population, but also some rostral ipsilateral pRS neurons. Note the axons of the contralateral pRS neurons crossing the midline in C3.

Figure 5. 3D reconstructions of pRS neurons labeled differentially from different white matter zones.

Four 3D reconstructions, one for each tracer application employed (VF+LF, Zones 1-3), generated using the Neurolucida Solids modeling module. Ipsilateral pRS neurons are blue, contralateral pRS neurons are green, and other neurons (including vestibulospinal and medullary reticulospinal) are grey. The surface of each reconstruction (transparent white) has been generated from section outlines. In the VF+LF reconstruction, contralateral pRS neurons are concentrated in the caudal portion of the pons, whereas the ipsilateral pRS population is larger and more evenly distributed along the rostrocaudal axis. In the Zone 1-3 reconstructions, ipsilateral pRS neurons are mainly labeled from Zones 1 and 2, whereas contralateral pRS neurons are mainly labeled from Zone 3.

Figure 6. Regional variation of pRS neuron soma size

A) Image of retrogradely labeled ipsilateral neurons and axons, including the ipsilateral pRS neurons and axons, from 4 adjacent parasagittal 50 µm sections (taken between 400 to 600 µm from the midline) projected onto a single layer. The ipsilateral pRS population can be seen as a continuous band of labeled neurons that starts around the pons/medulla transition (horizontal line of tick-marks, 100 µm intervals) and that follows the natural curvature of the pons rostrally. It thus extends from the PnC to the PnO, which we have operationally defined as respectively caudal and rostral to the oblique, dotted line. Clusters of neurons that were not considered part of the pRS are also labeled, including those in the nucleus subcoreuleus alpha and dorsal (SubCA/D), Barrington´s nucleus (Bar) and the medial vestibulospinal nucleus, parvocellular part (MVePC). The genu of the facial nerve can be seen as a dark spot (arrowhead) to the left of the vertical line of tick-marks (100 µm intervals) that has been used as the rostrocaudal axis in all figures. The circled cross indicates the intersection of the vertical and the dorsoventral axes and represents the origin of both, used in the graphs presented in other figures. **B)** Image of retrogradely labeled contralateral neurons and axons, including the contralateral pRS neurons and axons, from 4 adjacent parasagittal 50 µm sections (taken from 600 to 800 µm from the midline) projected onto a single layer. Axes and division between PnC and PnO as in A. Also labeled are neurons in the medial vestibulospinal nucleus, magnocellular part (MVeMC). **C-E**: Graphs displaying soma sizes of pRS neurons (magenta: ipsilateral, green: contralateral) measured in the parasagittal plane in 100 µm bins along the rostrocaudal axis (C), mediolateral axis (D) and dorsoventral axis (E). Circles indicate mean values and error bars represent standard deviations.

Figure 7. pRS neuron density along the rostrocaudal axis.

Graph showing density of ipsilateral (magenta diamonds) and contralateral (green circles) pRS neurons measured in 100 µm-on-a-side cubes along the rostrocaudal axis. Densities averaged below 5 neurons/10^6 µm^3 but could reach as high as 10 neurons/10^6 µm^3. For example, the single highest density (the magenta diamond within the 600-700 µm bin) matches well the densely populated area indicated by the open arrow in Figure 2B.

Figure 8. Distribution of putative GABAergic neurons among the pRS neurons.

Collapsed confocal image stacks of 14µm transverse sections from the rostral PRF (four left images) and caudal PRF (two right images). Retrograde labeling was performed in GAD67 (top row) and GIN (bottom row) GFP reporter mice. Green: GAD67 or GIN expressing cells. Magenta: ipsilateral or contralateral pRS neurons (ipRS, cpRS). Note that GFP+ neurons within the PRF are much more numerous in GAD67 than in GIN reporter mice, a presumed consequence of the differences in the subtypes of putative GABAergic neurons that express GFP in these two transgenic mouse strains. In neither strain did we find pRS neurons that were positive for GFP.

Figure 9. pRS axon trajectories within the brainstem.

Collapsed confocal image stacks of 50 µm sections, showing pRS neurons and their axon trajectories. **A)** Oblique longitudinal section cut at an angle of approximately 35° to the parasagittal plane, showing caudal ipsilateral pRS neurons and their axons. **B)** Parasagittal section showing rostral ipsilateral pRS neurons and their axons. Arrowheads indicate the sharp 90° turns made by the axons as they begin their descent toward the spinal cord. **C, D)** Transverse sections showing ipsilateral pRS neurons and their axons, with color-coding for rostrocaudal depth within the section (blue is rostral, red is caudal). Examples can be seen of pRS axons that traverse much of the image within the same plane (constant color) before turning abruptly (changing color rapidly, arrowheads) and leaving the section. **E)** Oblique transverse section through the rostral pons (oriented radially from ventricular to pial surface according to the curvature of the pons) showing contralateral pRS neurons and their axons. Several individual axons can be followed for different distances dorsally and then medially within the same transverse plane (constant color) before crossing the midline and beginning their descent toward the spinal cord. Scale bars as indicated.

Figure 10. Summary figure.

Cartoon illustrating some of the major findings in this study. Ipsilateral and contralateral pRS neuron populations (ipRS, blue, and cpRS, green) are drawn as shapes that roughly represent their relative positions and neuron numbers. IpRS neurons are numerous at all rostrocaudal levels, whereas cpRS neurons are more numerous in the rostral than the caudal pons. The relative distributions of ipRS and cpRS axons in the three zones of the white matter are indicated by color saturation with the darkest and lightest colors indicating highest and lowest number of axons, respectively.

Supplementary Figure 1. Spatial relationship between the ipsilateral and contralateral pRS neuron populations. Raw data from two separate preparations.

This figure compares the two preparations contributing to Figure 3, the data from each shown in different colors. The two data sets showed very similar distributions. The figure organization mirrors that of Figure 3, with some exceptions: 1) The ipsilateral and contralateral preparations have been separated – in A and C by showing them in their actual positions, on opposite sides of the midline, and in B and D, with side views of each laterality shown in separate diagrams; 2) Neuron positions are shown as raw data, in which the mediolateral resolution is limited to 50μm corresponding to the thickness of the parasagittal sections. In Figure 3, the positions were randomized within each 50μm interval, to eliminate the distracting stripes and to better show variations in density.

Tables

Table 1. Antibodies used in this study

Antibody name	Type	Host species	Dilution	Company	Cat. nr.	RRID	Specificity
Tetramethylrhodamine	Polyclonal	Rabbit	1:1000	Invitrogen	A-6397	AB 1502299	Quenches >50% of tetramethylrhodamine fluorescence. Cross-reactivity with Texas Red and Rhodamine Red dyes.
Pan-neuronal Neurofilament	Monoclonal	Mouse	1:5000	Covance	SMI-311R-100	AB 10143907	Non-phosphoneurofilaments, mammalian.
Alexa 555 goat-anti-rabbit	Polyclonal	Goat	1:400	Invitrogen	A21428	AB 141784	Rabbit IgG, H+L chains.

Table 2. Number of labeled ipsilateral and contralateral pRS neurons

Estimates from size analysis			Estimates from 3D reconstructions								
	VF+LF			**VF+LF**		**Zone 1**		**Zone 2**		**Zone 3**	
	Prep. A; Prep. B			Mean +/- SD		Prep. A; Prep. B					
Laterality	Ipsi	Contra		Ipsi	Contra	Ipsi	Contra	Ipsi	Contra	Ipsi	Contra
Above line	459; 214	167; 181	PnO	376 +/- 65	184 +/- 70	240; 240	48; 6	174; 144	84; 54	54; 90	198; 180
Below line	403; 282	42; 59	PnC	352 +/- 70	28 +/- 23	528; 420	30; 0	108; 144	30; 6	12; 0	54; 18
Sum	862; 496	209; 240		728 +/- 49	212 +/- 56	768; 660	78; 6	282; 288	114; 60	66; 90	252; 198

Sivertsen et al. Figure 1

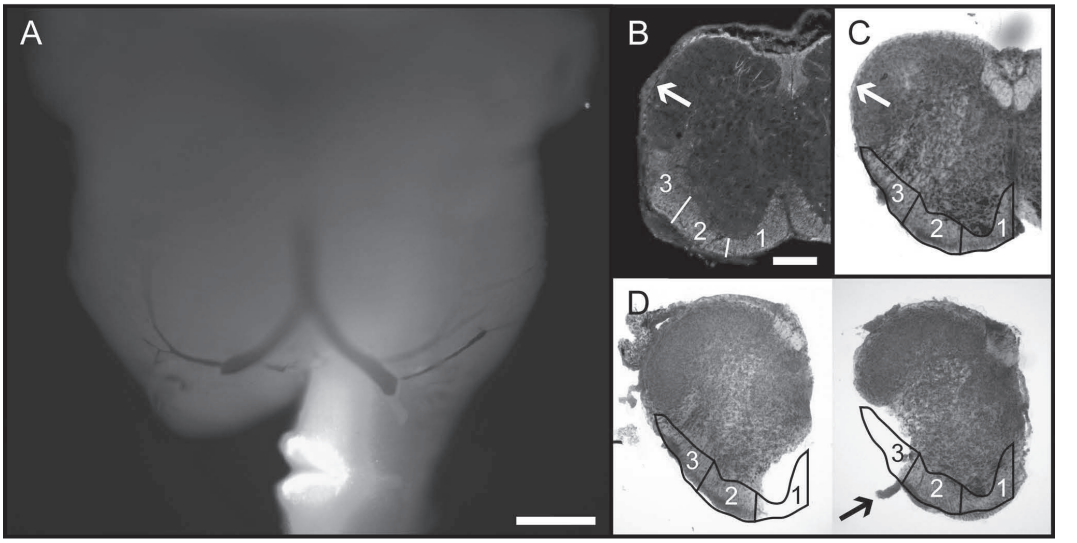

Sivertsen et al. Figure 2

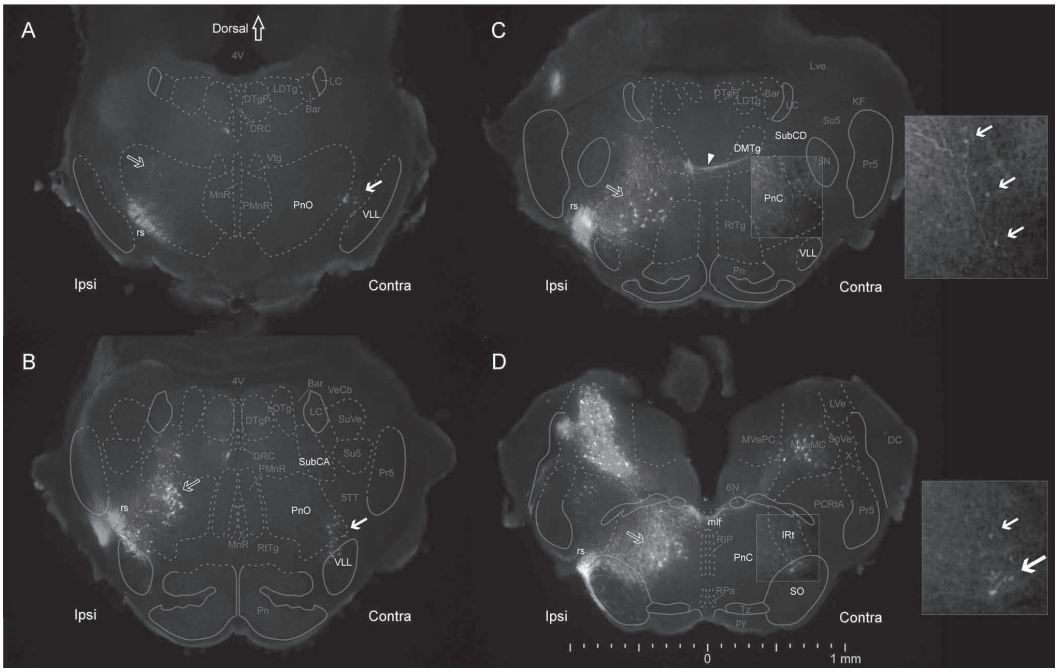

Sivertsen et al. Figure 3

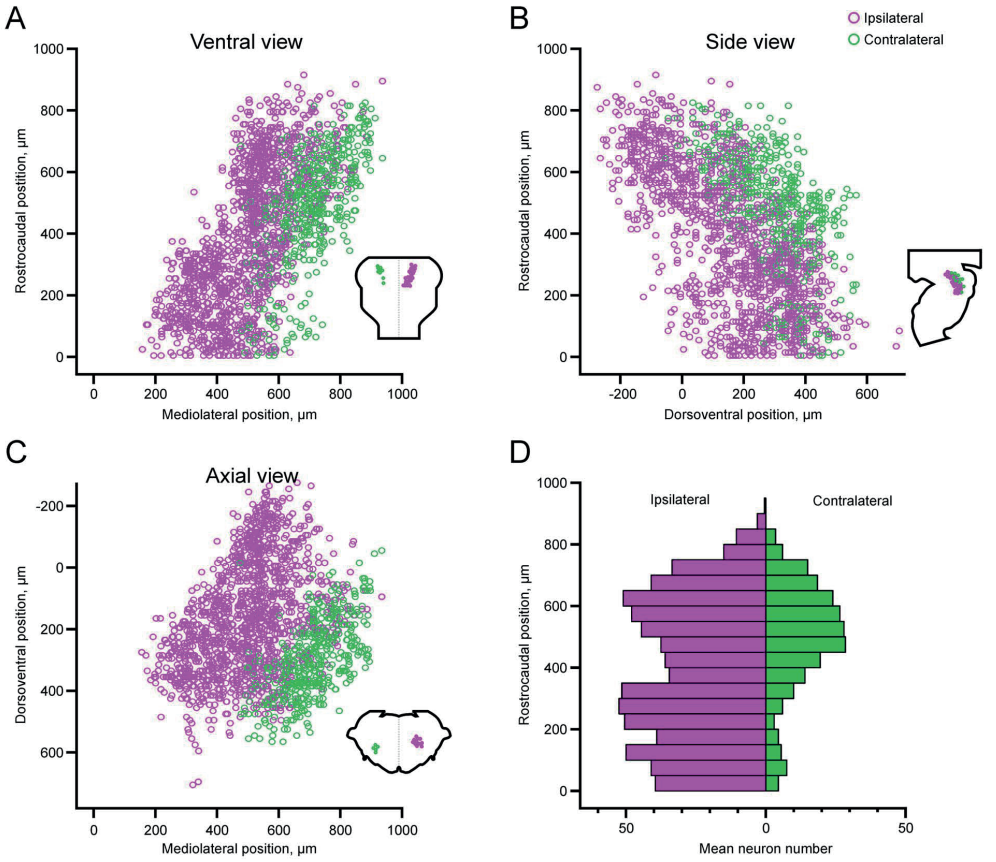

Sivertsen et al. Figure 4

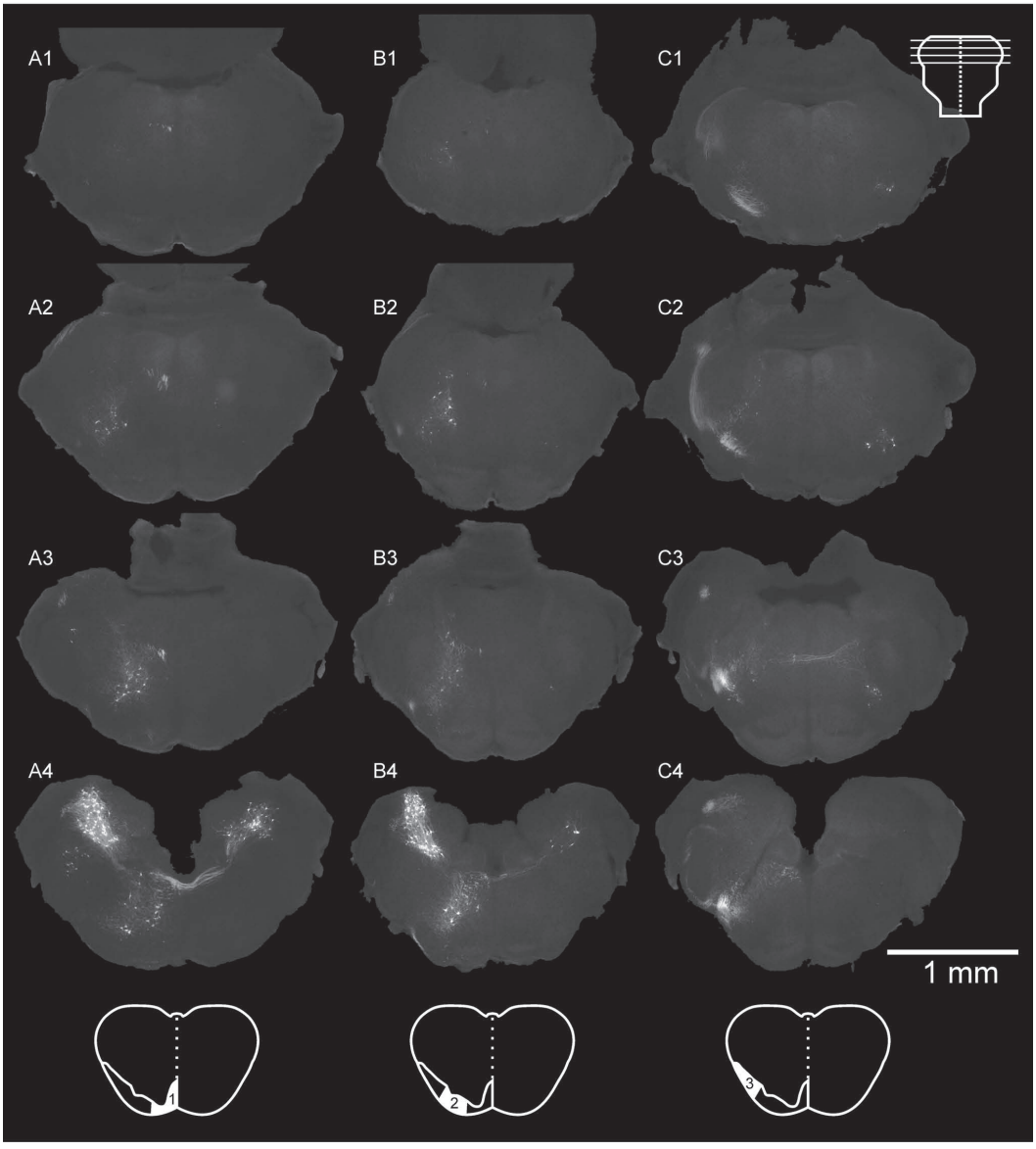

Sivertsen et al. Figure 5

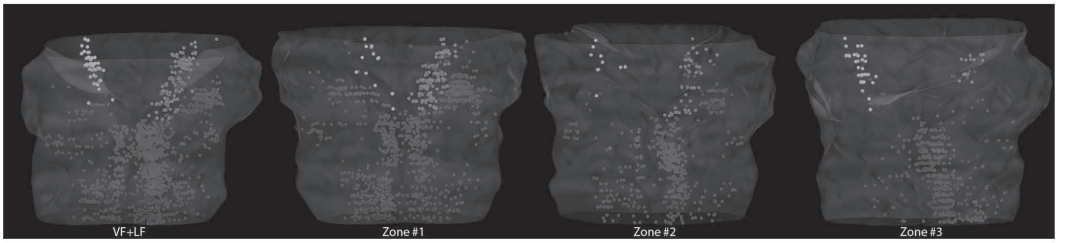

Sivertsen et al. Figure 6

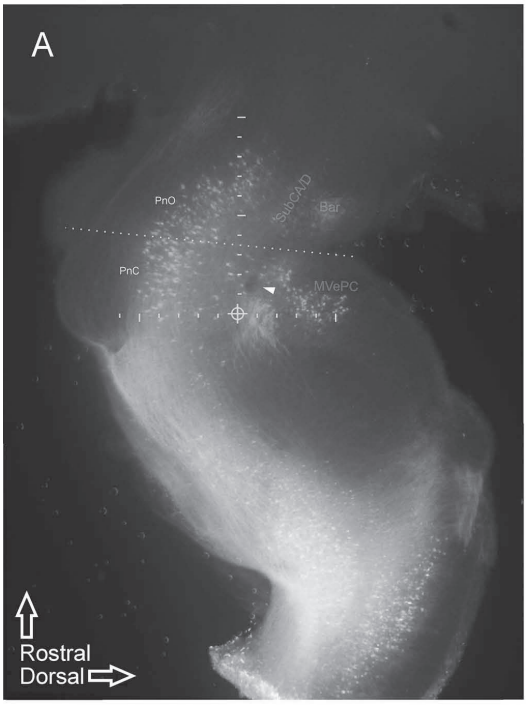

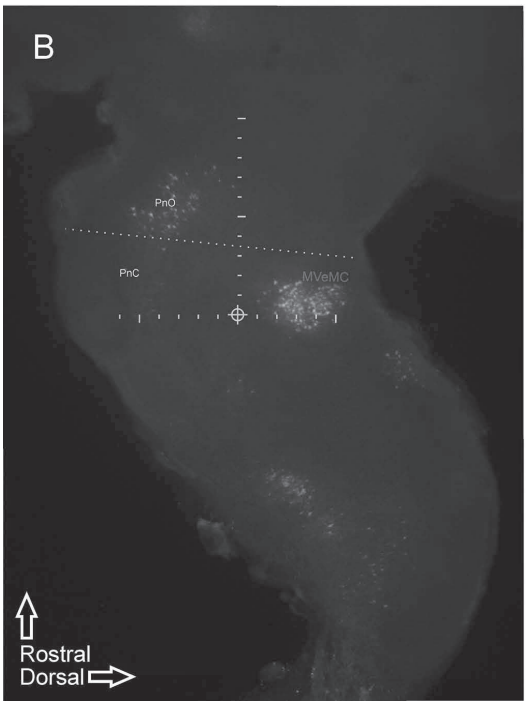

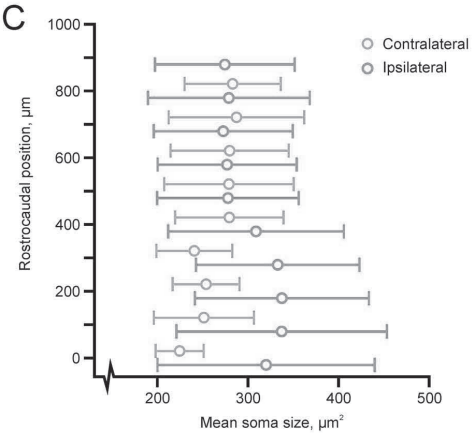

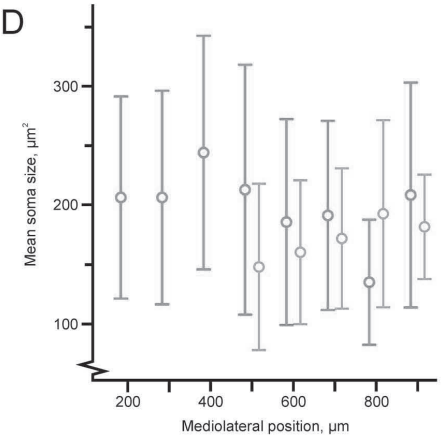

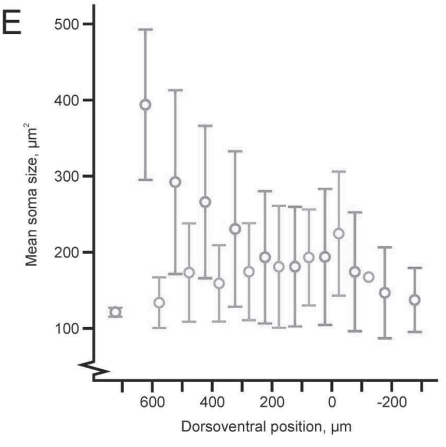

Sivertsen et al. Figure 7

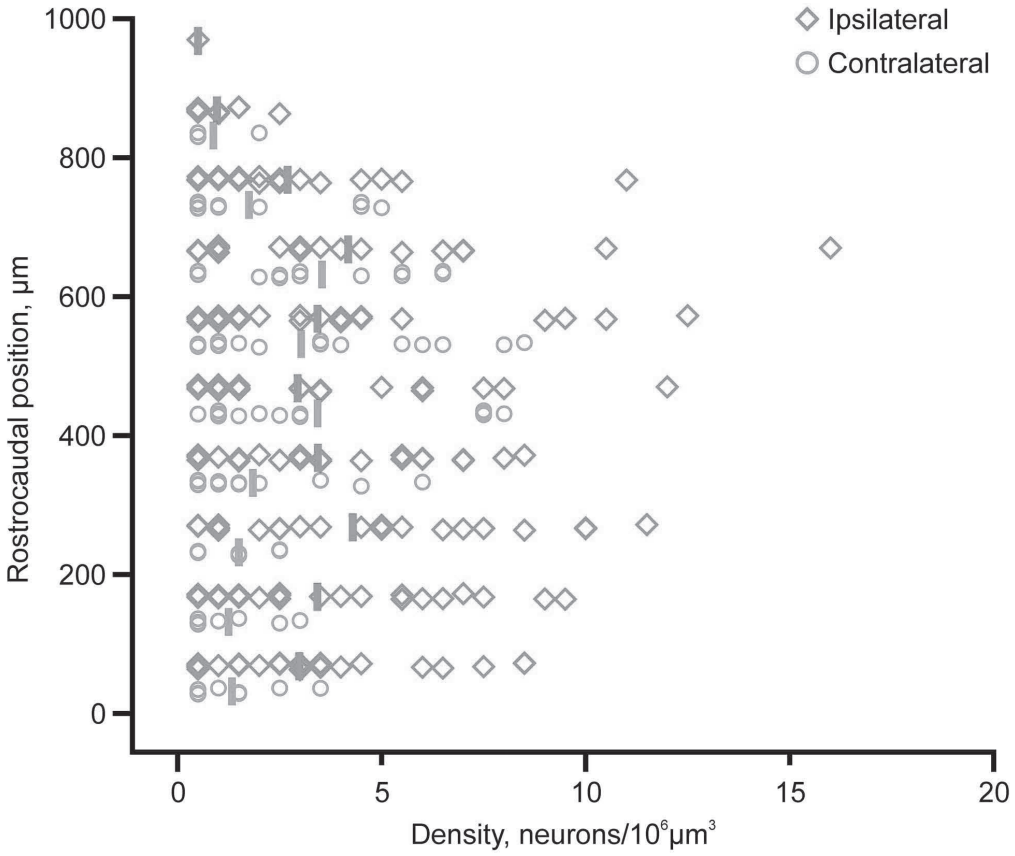

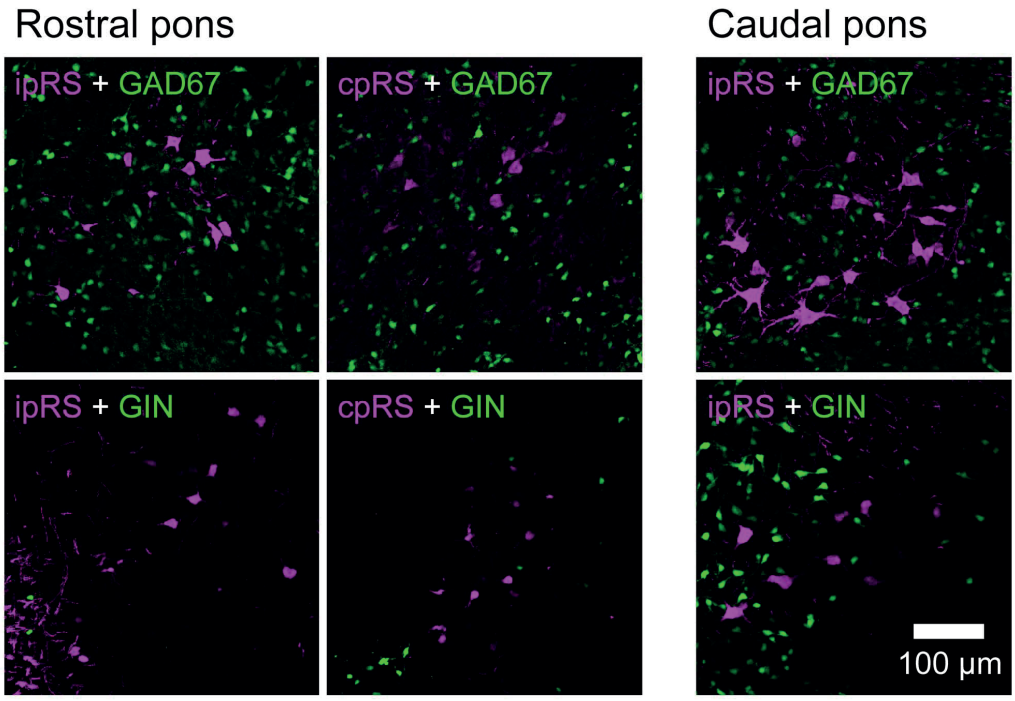

Sivertsen et al. Figure 8

Sivertsen et al. Figure 9

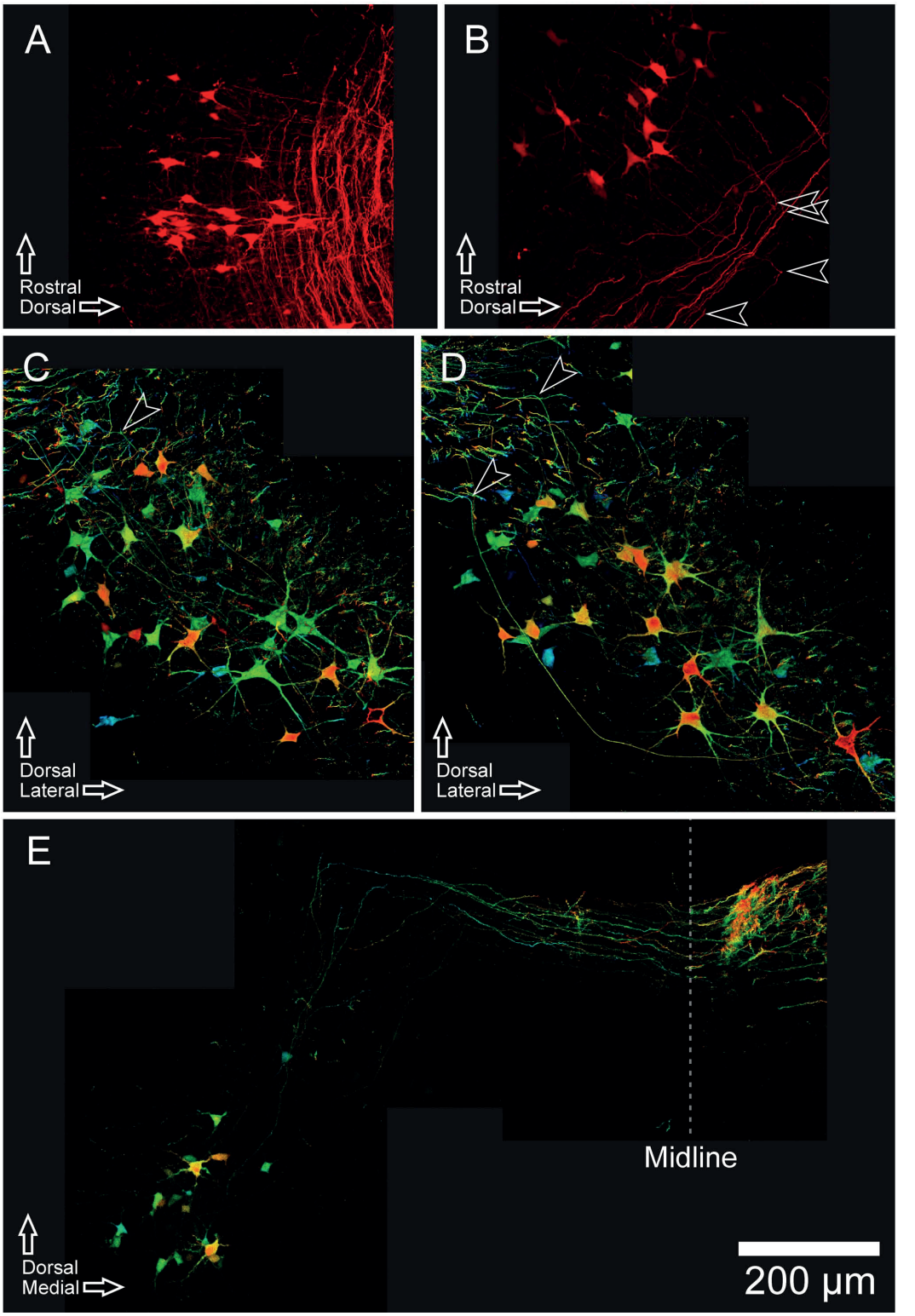

Sivertsen et al. Figure 10

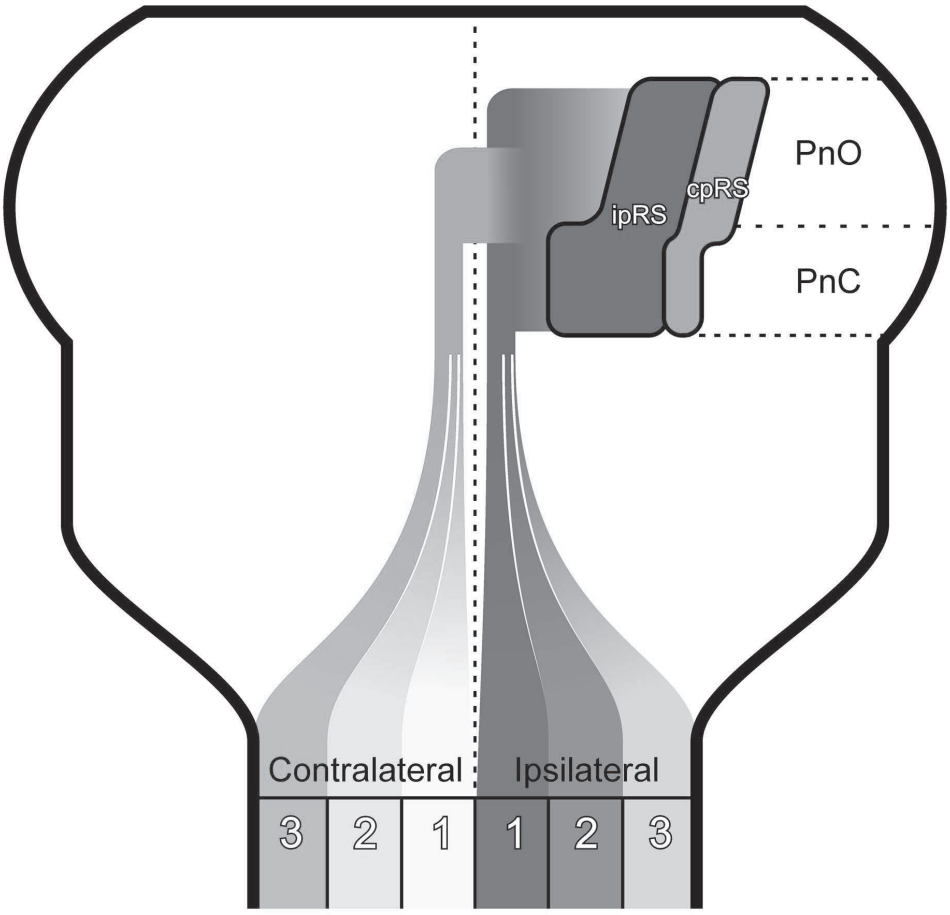

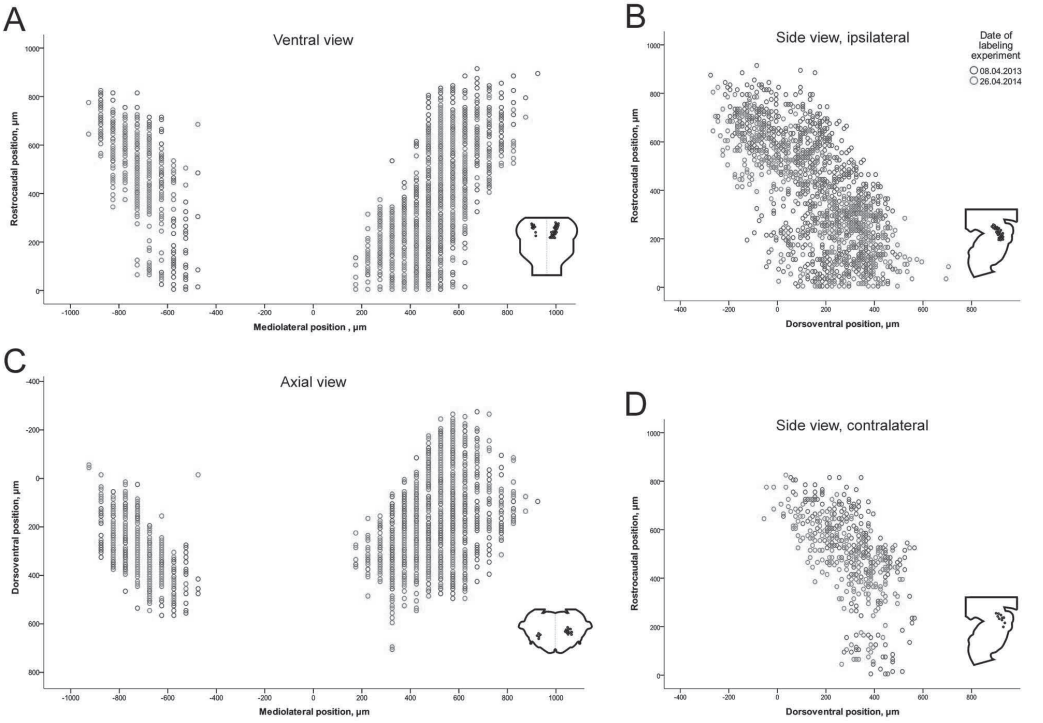

Sivertsen et al. Suppl. figure 1